12-2016

Fabrication of Infrared Photodetectors Utilizing Lead Selenide Nanocrystals

Justin Anthony Hill
University of Arkansas, Fayetteville

Fabrication of Infrared Photodetectors Utilizing Lead Selenide Nanocrystals

A thesis submitted in partial fulfillment
of the requirements for the degree of
Master of Science in Microelectronics-Photonics

by

Justin Hill
Henderson State University
Bachelor of Science in Physics, 2013

December 2016
University of Arkansas

This thesis is approved for recommendation to the Graduate Council.

Dr. Omar Manasreh
Thesis Director

Dr. Jingxian Wu
Committee Member

Dr. Rick Wise
Ex-Officio Member

Dr. Jiali Li
Committee Member

The following signatories attest that all software used in this thesis was legally licensed for use by Justin Hill for research purposes and publication.

_____ _____

Justin Hill, Student Dr. Omar Manasreh, Thesis Director

This thesis was submitted to http://www.turnitin.com for plagiarism review by the TurnItIn company's software. The signatories have examined the report on this thesis that was returned by TurnItIn and attest that, in their opinion, the items highlighted by the software are incidental to common usage and are not plagiarized material.

_____ _____

Dr. Rick Wise, Program Director Dr. Omar Manasreh, Thesis Director

Abstract

Colloidal lead selenide and lead selenide / lead sulfide core/shell nanocrystals were grown using a wet chemical synthesis procedure. Absorbance and photoluminescence measurements were made to verify the quality of the produced nanocrystals. Absorbance spectra were measured at room temperature, while photoluminescence spectra were measured at 77 K. Organic ligands were exchanged for shorter ligands in order to increase the conductivity of the nanocrystals. Absorption and PL spectra for both core and core/shell nanocrystals were compared. Interdigital photodetector devices with varying channel widths were fabricated by depositing gold onto a glass substrate. Lead selenide nanocrystals were deposited onto these metallic structures using drop casting. Current-voltage characterization was performed on these devices and showed approximately one order of magnitude enhancement in the photocurrent. The detectivity and responsivity were extracted from the current-voltage characterization.

Acknowledgements

I would like to express my gratitude to Dr. Omar Manasreh for supporting my research and always providing guidance when needed. His help and instruction was invaluable throughout this process.

I would also like to extend my gratitude to several members of my research group: Ahmad Nusir, Yahia Makableh, Juan Aguilar, and Ramesh Vasan. Each of them provided unique insights related to my research that helped me tremendously. In addition, I am very grateful to Dr. Mourad Benamara for his assistance with imaging of my materials.

I offer special thanks to Haley Morris for her aid, encouragement, and friendship during this period.

Dedication

This thesis is dedicated to my parents who have always supported me in everything I do, and to Amber Robbins for always believing in me, even when I did not believe in myself.

Table of Contents

Chapter 1: Introduction 1

1.1 Motivation 1

1.2 Relevance 2

1.3 Objectives 2

Chapter 2: Background 4

2.1 Review of Nanostructures 4

2.2 Photodetector Basics 10

2.3 Literature Review 12

Chapter 3: Research 18

3.1 Equipment 18

3.2 PbSe Nanocrystal Synthesis 19

3.3 PbSe Nanocrystal Characterization 20

3.4 PbSe Photodetector Fabrication 25

3.5 PbSe/PbS Core/Shell Nanocrystal Synthesis 38

Chapter 4: Conclusions and Future Work 45

4.1 Conclusions 45

4.2 Future Work 46

References 48

Appendix A: Description of Research for Popular Publication 51

Appendix B: Executive Summary of Newly Created Intellectual Property 53

Appendix C: Potential Patent and Commercialization Aspects of Listed Intellecutal Property Items 54

Appendix D: Broader Impact of Research 55

D.1 Applicability of Research Methods to Other Problems 55

D.2 Impact of Research Results on U.S. and Global Society 55

D.3 Impact of Research Results on the Environment 56

Appendix E: Microsoft Project for MS MicroEP Degree Plan 57

Appendix F: Identification of All Software Used in Research and Thesis 58

Appendix G: All Publications Published, Submitted and Planned 59

List of Figures

Figure 2.1.1. Illustration of interband transitions in a nanostructure 6

Figure 2.1.2. The three most common epitaxial growth modes are (a) Frank-van der Merwe growth, (b) Stranski-Krastanov growth, and (c) Volmer-Weber growth [15]. 9

Figure 2.3.1. The effective band gap of a semiconductor nanostructure is dependent on its size. The effective band gap of cadmium sulfide nanostructures is plotted as a function of radius [18]. 12

Figure 2.3.2. Device structure detailed in [21]. 13

Figure 2.3.3. Tang et al. fabricated this photodetector structure in [10]..... 14

Figure 2.3.4. In [4], the time-resolved photocurrent of a photodetector was presented. The photodetector was placed at a bias voltage of 120 V. 15

Figure 2.3.5. Photoluminescence spectra were obtained for lead selenide / cadmium selenide core/shell nanocrystals of varying core and shell sizes [22]. 16

Figure 2.3.6. Lead selenide and lead selenide / cadmium selenide core/shell nanocrystals were imaged with transmission electron microscopy in [22]. 17

Figure 3.1.1. A Schlenk line configuration was used for nanocrystal synthesis. 18

Figure 3.3.1. The absorbance spectrum for lead selenide nanocrystals dispersed in chloroform is shown. Nanocrystals were grown at 140 oC for 20 seconds. 21

Figure 3.3.2. Transmission microscopy imaging was performed on the lead selenide nanocrystals..... 22

Figure 3.3.3. Energy-dispersive X-ray spectrum for lead selenide nanocrystals..... 23

Figure 3.3.4. The photoluminescence spectrum was obtained for lead selenide nanocrystals grown at 140 ^{o}C for 20 seconds. 24

Figure 3.4.1. An interdigital photodetector contact structure was chosen for this research. 25

Figure 3.4.2. Gold contacts were deposited on a glass substrate in an interdigital pattern. Structures with 20 µm and 50 µm channels were fabricated. 26

Figure 3.4.3. Absorbance spectra were obtained for three different concentrations of lead selenide nanocrystals capped with mercaptoacetic acid. 27

Figure 3.4.4. Lead selenide nanocrystals with mercaptoacetic acid ligands were added to an interdigital contact structure. Current-voltage characterization was performed. 28

Figure 3.4.5. Responsivity of the photodetector was calculated from the current-voltage characteristics. 29

Figure 3.4.6. Specific detectivity was calculated using the responsivity and current-voltage characteristics. 30

Figure 3.4.7. Current-voltage characterization was performed after five dips in ethanedithiol. .. 32

Figure 3.4.8. Current-voltage characterization was performed after 10 dips in ethanedithiol. 32

Figure 3.4.9. Current-voltage characterization was performed after 15 dips in ethanedithiol. 33

Figure 3.4.10. A photodetector with a 50 μm channel filled was dipped in ethanedithiol and lead selenide nanocrystals 10 times. The responsivity was calculated from the current-voltage characteristics in Figure 3.3.8. 34

Figure 3.4.11. A photodetector with a 50 μm channel filled was dipped in ethanedithiol and lead selenide nanocrystals 10 times. The specific detectivity was calculated from responsivity in Figure 3.4.10 and the current-voltage characteristics in Figure 3.4.8. 35

Figure 3.4.12. Spectral response was measured for 20 μm and 50 μm photodetectors with mercaptoacetic acid-capped nanocrystals. 36

Figure 3.4.13. Spectral response was measured for the 50 μm photodetector with ethanedithiol-capped nanocrystals. Measurements were performed at room temperature with a 5 V bias. 37

Figure 3.5.1. Lead selenide nanocrystals were synthesized. A lead sulfide shell was grown around the nanocrystals to create a core/shell structure. Lead sulfide has a larger band gap than that of lead selenide. 39

Figure 3.5.2. The absorbance spectra were obtained for lead selenide / lead sulfide core/shell nanocrystals. 41

Figure 3.5.3. The photoluminescence spectra of lead selenide / lead sulfide core/shell nanocrystals was obtained. Measurements were performed at 77 K. 42

Figure 3.5.4. Lead selenide / lead sulfide core/shell nanocrystals were imaged with high resolution transmission electron microscopy. 43

Chapter 1: Introduction

1.1 Motivation

Photodetectors are used for many applications including fiber optic communications [1], infrared imaging [2], solar monitoring [3], fire detection systems [4], astronomical observations [4], missile defense systems [4], and many more. These devices are vital in almost any instance where light is used as part of a system. Improving the response of these devices would increase the speed of telecommunications and increase light-sensing capabilities. In addition, many of the concepts that are associated with photodetectors are related to other optoelectronic devices such as solar cells and light emitting diodes. These improvements would have massive implications for society by increasing the bandwidth and speed of data transmissions as well as providing new technological insights for other applications [5], [6].

The potential for discovery would also be greatly increased, providing telescopes and detection arrays that can gather much more data about the universe. With the increased societal focus on space exploration, this type of information would be crucial. With improved sensing capabilities, exploratory probes would be able to locate many more fascinating stellar phenomena. One very recent example of this is the New Horizons probe, which recently passed near Pluto. Using X-ray sensors on the probe, scientists were able to learn many new things about Pluto and Charon: both bodies have partially active surfaces, there is evidence of active and standing water on Pluto, Pluto's atmosphere is far thicker than previously believed, and Charon may have a massive water-ice ocean inside of it [7]. All of these discoveries rely on optical sensors such as photodetectors. Improving these sensors will increase the amount of data that can be collected as well as improve the quality of said data.

1.2 Relevance

This work details the creation of an infrared photodetector using colloidal lead selenide nanocrystals. This approach produces a photodetector with high detectivity and responsivity. Furthermore, the cost of producing this type of detector is lower than that of a traditional photodetector as it does not require a P-N junction [8]. Unlike traditional photodetectors, the devices detailed in this work may be built on a simple glass substrate instead of silicon or some other semiconductor crystal.

The chemical synthesis procedure used in this work to create colloidal nanocrystals can be easily modified to allow for large scale production that would be required in industry. In addition, this synthesis uses non-vacuum systems in fabrication. This reduces the complexity of the operation as well as the cost.

The primary advantage of this type of device is that it should not require cooling to operate. Current infrared detectors require cooling systems to produce reliable, noise-free signals [9]. These systems are expensive, bulky, and costly to operate [9]. Detectors that operate at room temperature offer a low cost alternative to these systems. Because of their ability to operate at much higher temperatures, these devices are not as susceptible to fluctuations in environmental conditions.

1.3 Objectives

The goal of this research was to build an infrared light detecting device that would function at room temperature using colloidal lead selenide nanocrystals as well as lead selenide /

lead sulfide core/shell nanocrystals. This was done to compare the performance of these two types of structures. For this work, a detector with specific detectivity of at least 10^8 Jones was considered a success as reported in literature [10].

Chapter 2: Background

2.1 Review of Nanostructures

Quantum structures have garnered a great deal of interest in recent years. These novel materials could become the basis for the next generation of optoelectronic devices due to the unique properties that arise because of their dimensionality. Because the size of this type of material is extremely restricted in at least one direction, quantum effects yield properties that are not present in conventional materials. Of these properties, band gap tunability is perhaps the most commonly studied and utilized. This property allows the band gap of the material to be adjusted by altering the size of the nanostructures. Because of this effect, devices created with these materials are able to function outside of the range normally allowed by their respective bulk materials. This work focuses on the use of lead selenide nanocrystals and their use in infrared photodetectors. Using colloidally synthesized lead selenide nanocrystals, the band gap can be shifted from the mid infrared to near infrared. Lead selenide is a group II-VI binary semiconducting material with a direct band gap. Unlike many common semiconductors that are arranged in a zincblende/diamond or wurtzite structure, lead selenide is made from cubic unit cells [11].

In normal bulk semiconductors, there are billions of individual atoms. Each atom has identical discrete allowable energy states that electrons may occupy. When bonding with each other, the electron orbitals of each of these atoms interact with those around it [12]. This results in slightly altered energy states for each atom [12]. When this happens, there are billions of different possible energy states which causes the formation of bands of allowable energies [12]. In reality, these bands are actually made from discrete energy levels rather than a continuous range, however they are often considered to be continuous because the differences in energy are

miniscule [12]. In quantum structures, the size of the material is limited in one, two, or even three dimensions. This results in fewer allowable energy states in the limited dimension(s), thus forming quantized energy levels rather than bands. These energy levels are inversely proportional to the square of the size of the structure and are often modeled as an infinite potential well. The energy levels can be approximated as follows:

$$E_n = \frac{n^2 \hbar^2 \pi^2}{2m^* d^2} \qquad \text{(Equation 2.1)}$$

where E_n is the energy of the nth energy state, $\hbar$ is the reduced Planck constant, m^* is the effective mass of the electron in the material, and d is the size of the structure [13]. From Equation 2.1, it is easy to see that as the size of the structure decreases, the energies of the quantized levels increase. This results in an effective band gap that is larger than the band gap of the bulk material. This mechanism can be used to tailor the band gap of the structure to a desired quantity, thus allowing devices to be created for highly specialized functions. It can also be seen that the separation between the states corresponding to n = 1 and n = 2 is small compared to the separation between higher values of n. These energy differences correspond to interband transitions in the nanocrystals. Since there are several different energy states in the conduction and valence bands, there are a number of transitions that may occur. Generally, the transition between the highest valence state and the lowest conduction state is the strongest. This is because the coefficient of absorption is directly proportional to the oscillator strength of the transition [13]. The oscillator strength of a transition is given by

$$f_{vc} \approx \begin{cases} \left|1 - \frac{m_0}{m_e^*}\right| \; for\; electrons \\ 1 + \frac{m_0}{m_h^*} \; for\; holes \end{cases} \qquad \text{(Equation 2.2)}$$

where f_{vc} is the oscillator strength, m_0 is the mass of a free electron, m_e^* is the effective mass of the electron in the material, and m_h^* is the effective mass of the hole [13]. Due to parity, transition from odd to even or even to odd states (e.g., a transition from the first state in the valence band to the second state in the conduction band) is forbidden [13]. Figure 2.1.1 illustrates these different transitions.

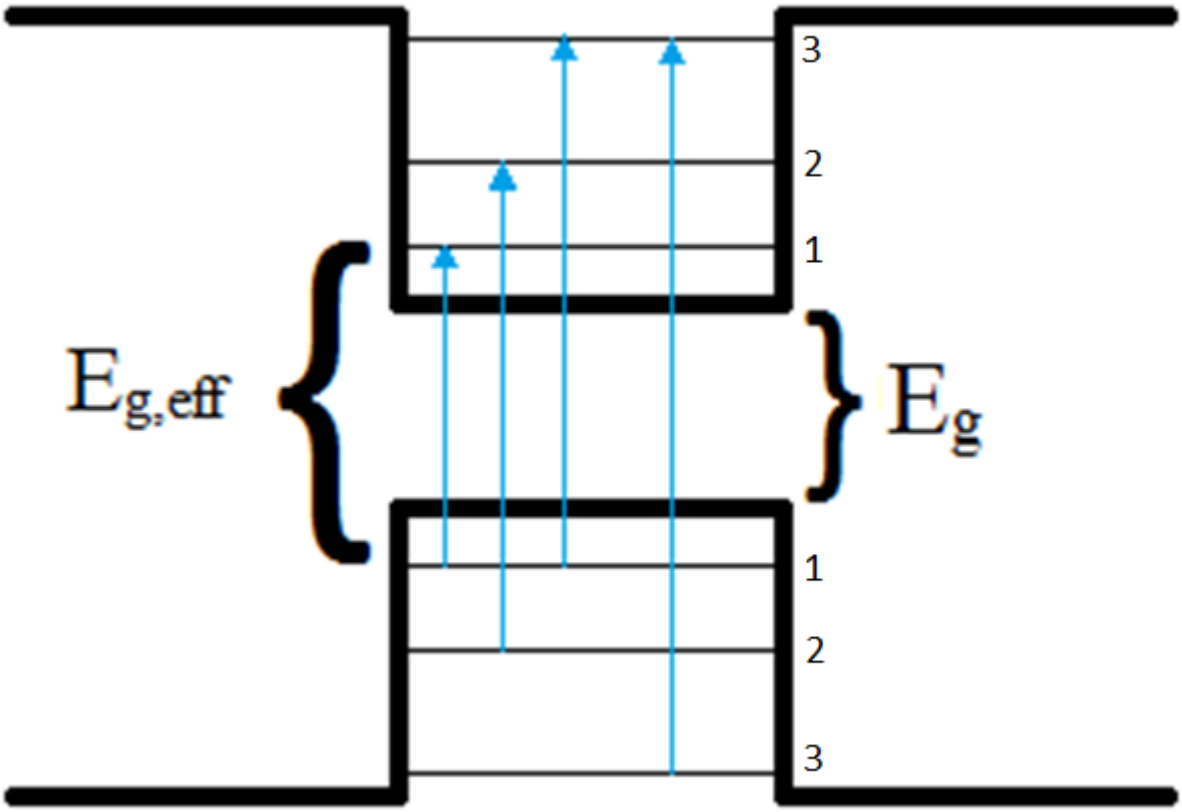

Figure 2.1.1. Illustration of interband transitions in a nanostructure

These quantum effects are most pronounced when the size of the structure is less than the Bohr exciton radius [14]. Excitons are a quasi-particle created when an electron is excited to the conduction band. When an electron is moved away from its parent atom, a positively charged nucleus is left behind. This positive "hole" can be compared to heavy traffic

flow. If a vehicle leaves a crowded highway, it leaves behind a hole. The car behind it will move forward to fill this hole, thus leaving another in its wake. In semiconductors, the positively charged hole and the negatively charged electron can become attracted to each other through coulomb interaction, similar to the binding of an electron to the proton in a hydrogen nucleus. This pair of interacting particles is referred to as an exciton. The radius of this bound pair is the Bohr exciton radius and is given by

$$a_{ex} = \frac{\varepsilon \hbar^2}{\mu e^2} \qquad \text{(Equation 2.3)}$$

where ε is the permittivity of the material and μ is the reduced effective mass of the electron and hole. Excitons may occur in two varieties: free excitons and bound excitons [13]. Free excitons are free to move around within bulk semiconductors [13]. Excitons become bound when trapped in a defect within a lattice or when the lattice itself is physically restrictive [13]. This is the case in quantum structures, where one, two, or even three-dimensional confinement is present.

For nanocrystals, the effective band gap will approach that of the bulk material as the size of the nanocrystal increases. This can be seen in the equation

$$E_g^* = E_g + \chi\left(\frac{\pi^2 \hbar^2}{2\mu^* d^2}\right) \qquad \text{(Equation 2.4)}$$

where E_g^* is the effective band gap of the nanocrystal, E_g is the band gap of the bulk material, χ is a numerical factor, μ^* is the reduced effective mass of the electron and hole in the material, and d is the diameter of the nanocrystal. In an ideal nanocrystal, χ is unity.

Another advantage of using nanocrystals instead of bulk material arises when discussing contributions from thermal effects. Bulk lead selenide has a very narrow band gap (approximately 0.27 eV). As a result, electrons can be easily excited by thermal contributions. This causes a great deal of noise in photodetectors that operate at room temperature. This means

that infrared detectors must often be drastically cooled to achieve a clean signal. This work details the creation of an infrared photodetector utilizing lead selenide nanocrystals that functions at room temperature.

According to Manasreh, several methods can be used to fabricate nanocrystals. The first method is referred to as epitaxial growth. The processes included in epitaxial growth include molecular beam epitaxy, chemical vapor deposition, and metal-organic chemical vapor deposition. Each of the aforementioned methods has advantages, but all share common growth modes. The first growth method is referred to as Volmer-Weber growth or, in more colloquial speech, island growth. This growth method involves depositing material onto a substrate to which it does not bond strongly. In this instance, the deposited material bonds strongly to itself, thus leading to the formation of clusters on the surface of the substrate. The second growth mode is called Frank-van der Merwe growth. This is often referred to as layer growth because the deposited material forms two-dimensional surfaces before growing vertically. This occurs because the material bonds more strongly with the substrate than with atoms of the same type. Once the initial layers are formed, the deposited material begins to form clusters to reduce strain in the material. The final growth mode is Stranski-Krastanov growth. This growth mode combines the two previously mentioned modes. After the first few layers are grown, the deposited material begins to favor island deposition [13]. These growth modes are shown in Figure 2.1.2 [15].

Nanocrystals can also be fabricated by colloidal growth. Nanocrystals formed by colloidal growth have the advantage of being very low cost compared to those created by epitaxial means [13]. In addition, colloidal nanocrystal synthesis procedures can be easily scaled up for mass production by simply adjusting the initial amounts of reactants. Because of the

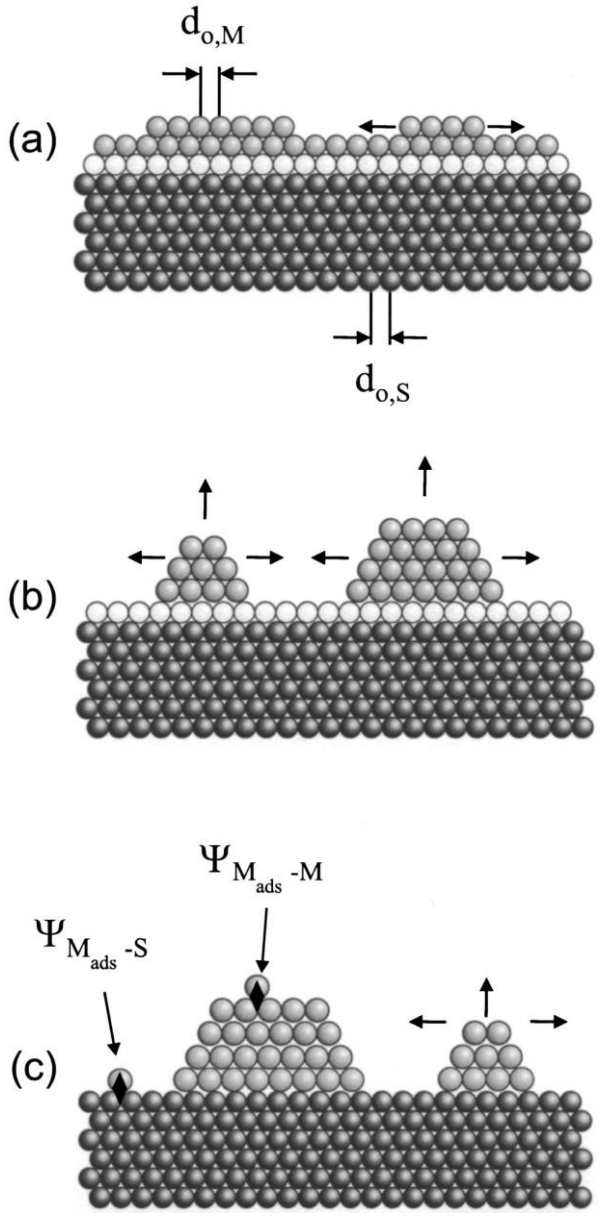

Figure 2.1.2. The three most common epitaxial growth modes are (a) Frank-van der Merwe growth, (b) Stranski-Krastanov growth, and (c) Volmer-Weber growth [15].

nature of colloidal synthesis, the size distribution of produced nanocrystals is typically larger than that of those created by epitaxial growth. Nanocrystals formed by colloidal synthesis procedures are usually suspended in a solution. This allows the usage of less costly deposition techniques such as drop casting, dip coating, or spin coating. Colloidal synthesis requires the use

of organic molecules known as ligands to protect and isolate the structures [13]. Without these ligands, nanocrystal aggregation may occur, resulting in a loss of the quantum effects for which they were synthesized. The initial ligands used have a large impact on the size of the produced nanocrystals [16]. Ligands are typically molecules made of carbon-hydrogen chains [16]. Ligands made from longer carbon-hydrogen chains are more likely to passivate the nucleation of the precursor chemicals, resulting in nanocrystals with smaller radii [16]. For this reason, long ligands are often used during colloidal synthesis procedures [16]. Exchange or complete removal of these ligands is often required due to the non-conductive nature of long ligand molecules [13].

2.2 Photodetector Basics

A photodetector is a device that is used to detect light within a specific range of wavelengths. This is done by providing an amplification in the current passing through the device when the incident light is within that range. Most photodetectors are placed at a certain bias voltage. The current that passes through the device when there is no incident light is referred to as the dark current. When light that is within the associated range is incident on the photodetector, electrons in the semiconductor material become excited and transition from the valence band to the conduction band. This causes the material to become more conductive due to the increase in free charge carriers. Because conductivity is inversely proportional to resistance, this means that the resistance in the device decreases. According to Ohm's law, a decrease in resistance in the presence of a constant voltage will produce an increase in current. This increased current due to the interaction of incident light with the semiconducting material in

a photodetector is called the photocurrent. Ideally, the ratio between the photocurrent and the dark current in a photodetector should be large. The difference between these two currents is not the only consideration, however. A photodetector with a high dark current will dissipate more power and will be costlier to operate.

Photodetectors are often evaluated according to their specific detectivity and responsivity. Responsivity in a photodetector can be thought of as a measure of the ratio of electrical output to optical input. A photodetector with high responsivity would be capable of producing a large photocurrent even when the intensity of the incident light is small. The specific detectivity is used as a figure of merit by which the performance of photodetectors with different sizes are compared. The responsivity of a photodetector can be determined by the following equation:

$$R = \frac{I_{PC}}{P} \qquad \text{(Equation 2.5)}$$

where R is the responsivity (A/W), I_{PC} is the photocurrent, and P is the incident light power. The specific detectivity is given by:

$$D^* = \frac{R\sqrt{A}}{\sqrt{2eI_{DC}}} \qquad \text{(Equation 2.6)}$$

where D^* is the specific detectivity (usually expressed in the Jones unit, $cm\sqrt{Hz}/W$), R is the responsivity, A is the active area of the device, e is the charge of an electron, and I_{DC} is the dark current. Nanocrystals are expected to produce devices with higher responsivity and specific detectivity than that of photodetectors utilizing traditional bulk semiconductor materials [17]. This makes nanocrystal photodetectors highly promising for advancing photodetection technology.

2.3 Literature Review

The size-dependent band gap of cadmium sulfide, cadmium telluride, cadmium selenide, and indium phosphide nanostructures were observed by Baskoutas et al. in [18]. For each material, energy was plotted as a function of radius. The energy-radius relationship for cadmium sulfide is shown in Figure 2.3.1.

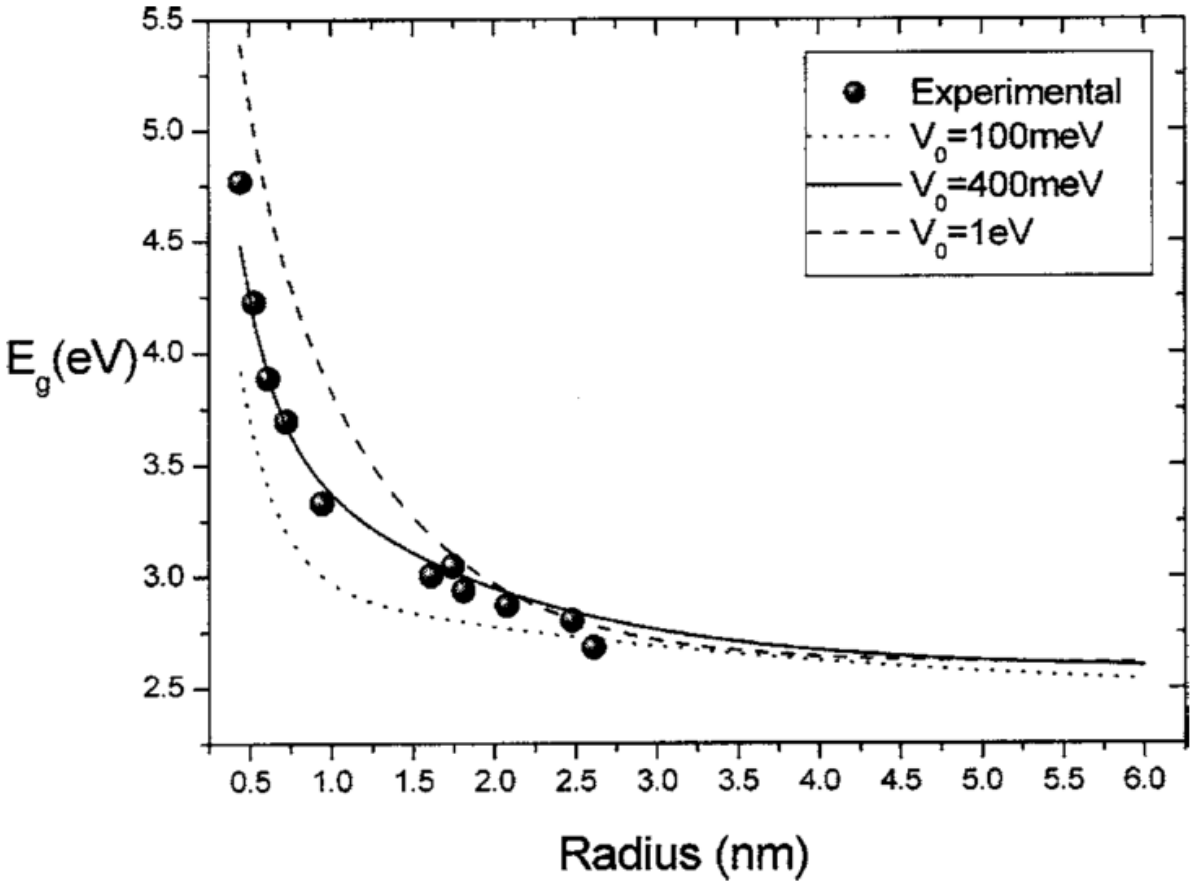

Figure 2.3.1. The effective band gap of a semiconductor nanostructure is dependent on its size. The effective band gap of cadmium sulfide nanostructures is plotted as a function of radius [18].

Bulk cadmium sulfide has a band gap of 2.482 eV [19]. As the radius of the material decreases, the energy of absorbed photons increases, doubling at approximately 0.5 nm. The Bohr exciton radius of cadmium sulfide is 5.8 nm [20]. At this point in Figure 2.3.1, the effective band gap of the nanostructures is similar to that of bulk cadmium sulfide.

Lead selenide nanocrystals were synthesized and an absorbance peak was reported at approximately 1500 nm by Cui et al [21]. The lead selenide nanocrystals used were coated with oleic acid to isolate the nanocrystals and prevent aggregation. The author believes that the performance of the nanocrystals was limited due to the non-conductive nature of the oleic acid ligands. These nanocrystals were suspended in a polymer and used to create a photodetector with responsivity of 1.8×10^{-5} A/W. No value was given for the specific detectivity of the aforementioned detector. The device structure is shown in Figure 2.3.2 [21].

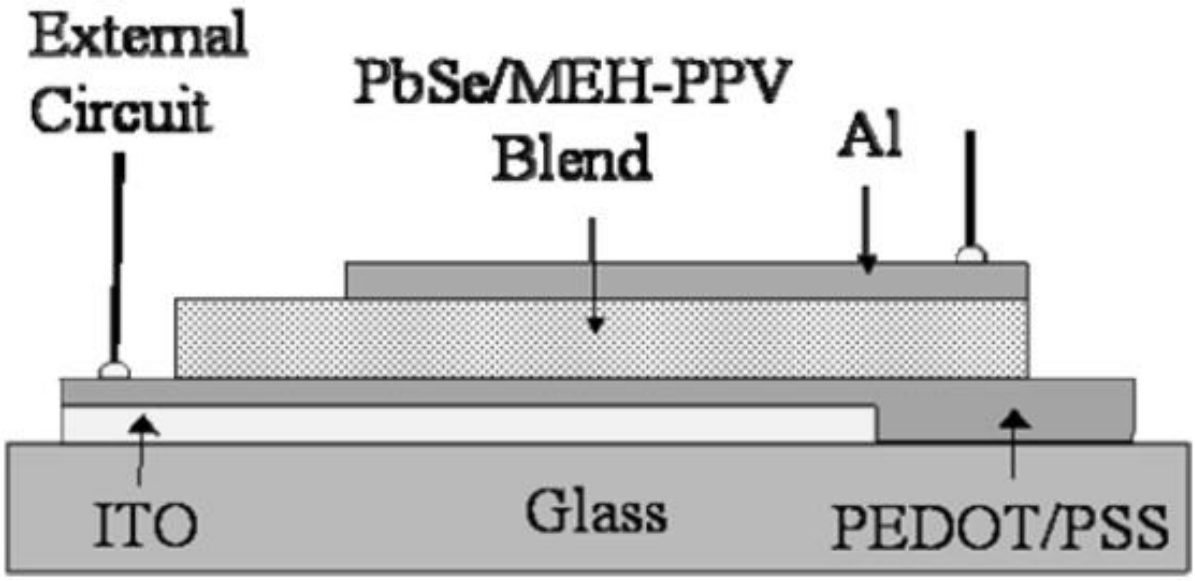

Figure 2.3.2. Device structure detailed in [21].

A near-room-temperature infrared photodetector was fabricated by Tang et al. from a combination of indium arsenide and gallium arsenide quantum dots using molecular beam epitaxy and the Stranski-Krastanov growth method [10]. When cooled to 36 K, the peak responsivity was reported as approximately 2.7×10^{-2} A/W at a wavelength of 3 μm. When measured closer to room temperature (250 K) however, the responsivity dropped to 2.5×10^{-3} A/W, over an order of magnitude lower. The structure of this device was far more complex than most photodetectors and is shown in Figure 2.3.3 [10].

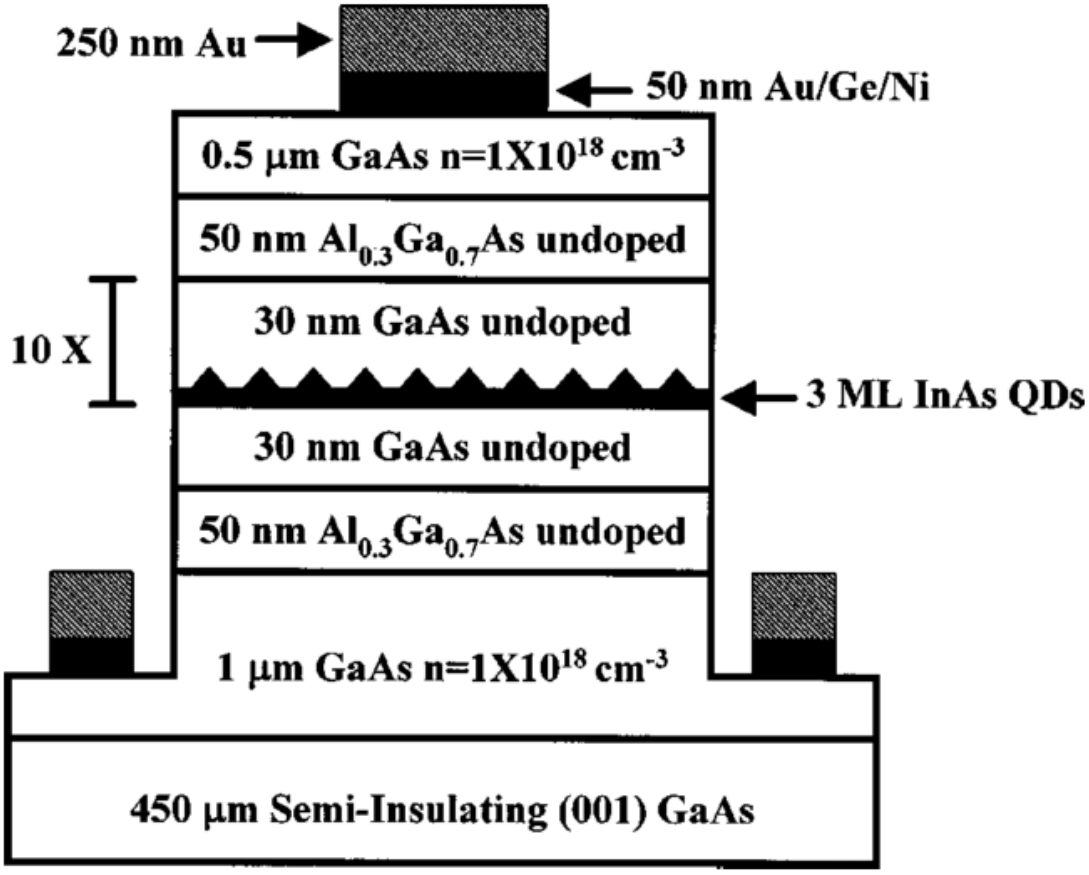

Figure 2.3.3. Tang et al. fabricated this photodetector structure in [10].

Nanocrystals can be used to make photodetectors for all wavelengths, not just infrared. Jin et al. report on the fabrication of an ultraviolet photodetector using colloidal zinc oxide nanocrystals [4]. This particular photodetector was reported to have a responsivity of 61 A/W. While this responsivity was high, the device suffered from a very low photocurrent (1 μA at a 5 V bias). The device also had a long relaxation time. The time-resolved photocurrent for this device after 25 seconds of exposure with a bias voltage of 120 V is shown below in Figure 2.3.4 [4].

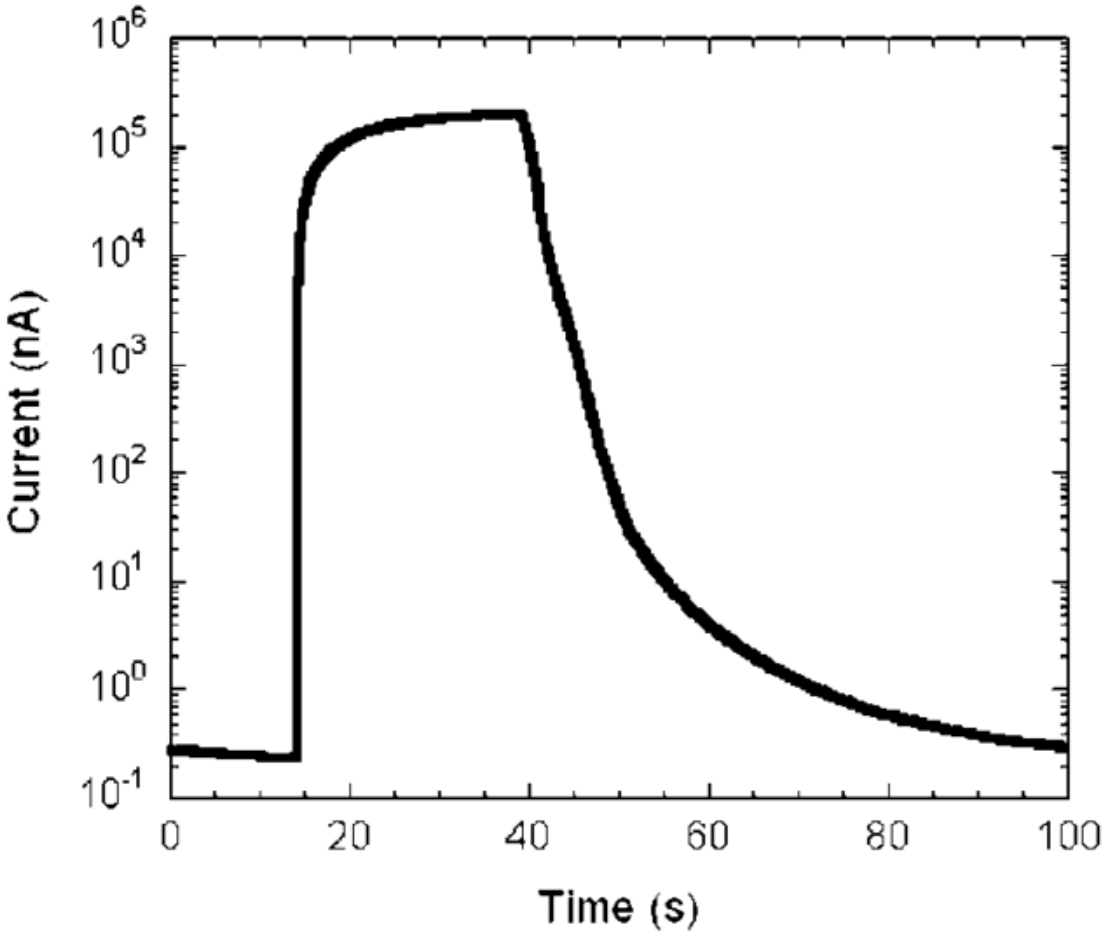

Figure 2.3.4. In [4], the time-resolved photocurrent of a photodetector was presented. The photodetector was placed at a bias voltage of 120 V.

Pietryga et al. reported on synthesis of lead selenide / cadmium selenide core/shell nanocrystals [22]. This structure was chosen due to degradation of lead selenide nanocrystals when exposed to ambient environmental conditions. Photoluminescence spectra were obtained for nanocrystals of varying core and shell sizes as shown in Figure 2.3.5 [22].

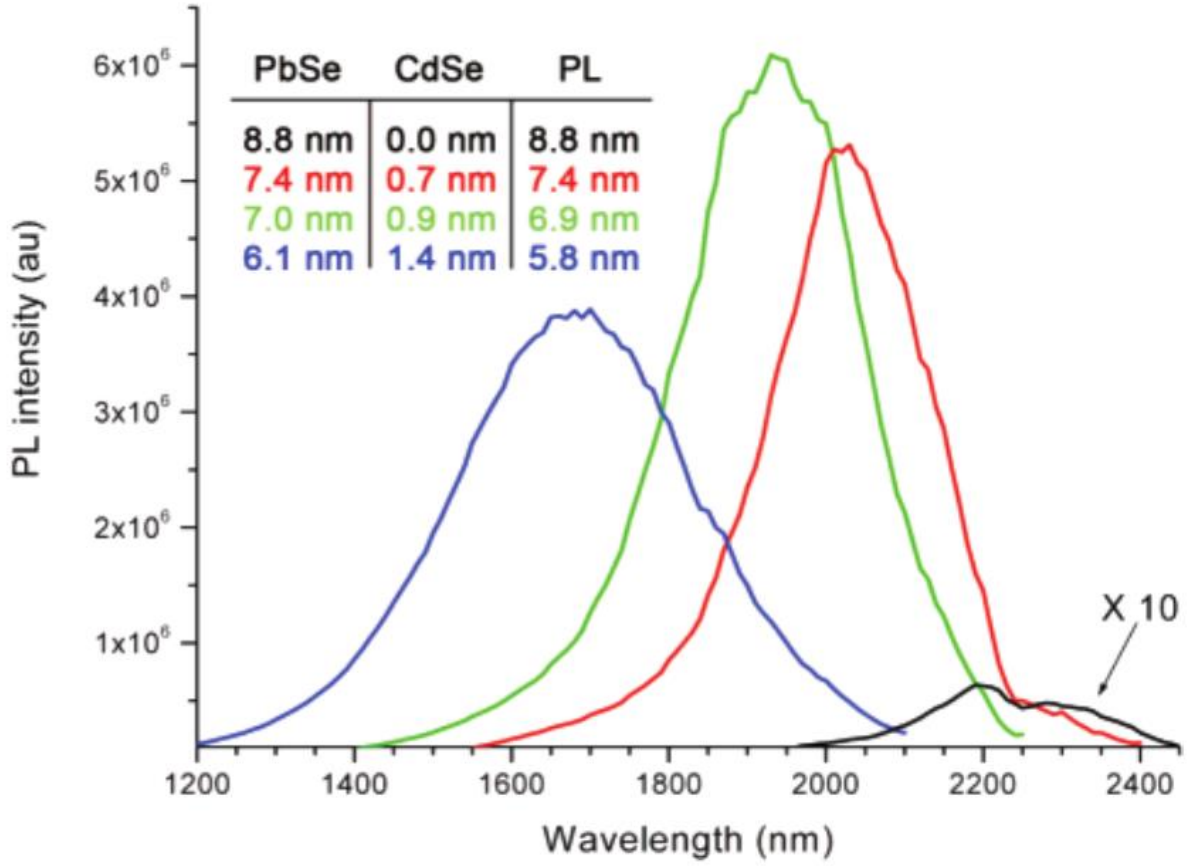

Figure 2.3.5. Photoluminescence spectra were obtained for lead selenide / cadmium selenide core/shell nanocrystals of varying core and shell sizes [22].

The photoluminescence column in the inset chart of Figure 2.3.5 is the size of the nanocrystal as predicted from the photoluminescence peak position. The black spectrum was obtained from basic lead selenide nanocrystals with no shell, while the red, green, and blue spectra were obtained for core/shell nanocrystals with growth times of 15 minutes, 2 hours, and

24 hours, respectively. Transmission electron microscopy images were obtained for lead selenide and lead selenide / cadmium selenide core/shell nanocrystals. In Figure 2.3.6, frame A shows lead selenide nanocrystals with a diameter of approximately 5 nm. In frames B and C, the interface between the lead selenide core and cadmium selenide shell can be clearly seen.

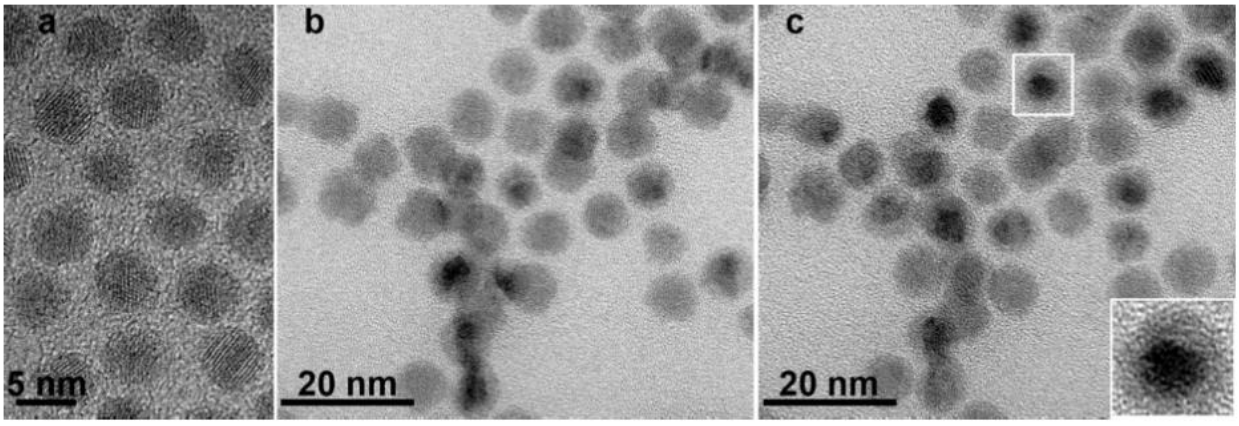

Figure 2.3.6. Lead selenide and lead selenide / cadmium selenide core/shell nanocrystals were imaged with transmission electron microscopy in [22].

Chapter 3: Research

3.1 Equipment

The equipment used in this work, with the exception of the FEI Titan high-resolution transmission electron microscope, is contained within Dr. Omar Manasreh's research lab at the University of Arkansas, Fayetteville. The equipment is as follows: a Cary 500 scan UV-Vis-NIR spectrophotometer, Bomem DA8 Fourier transform spectrometer, Bruker IFS 125 spectrometer, Keithley 4200 semiconductor characterization system, Angstrom Engineering Nexdep electron-beam physical vapor deposition system, Kulicke and Soffa model 4523 wire bonder, MTI PTL-OV5P dip coater, Labnet Hermle Z-300 centrifuge, Oakton Temp 5000 temperature controller, and a Schlenk line in the configuration shown below in Figure 3.1.1.

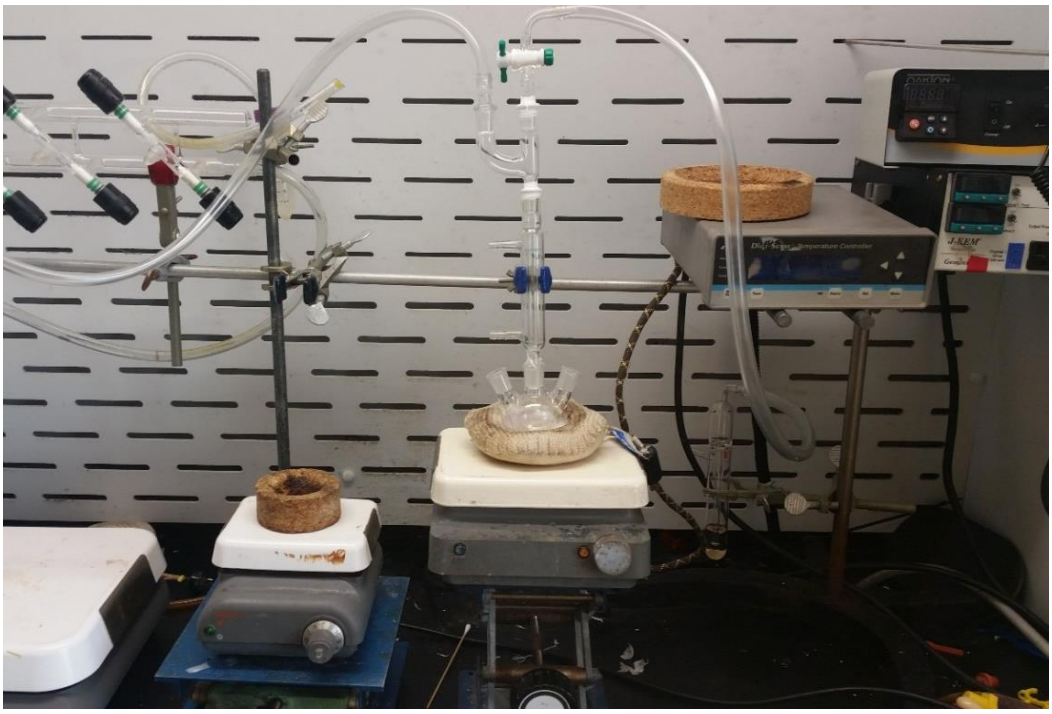

Figure 3.1.1. A Schlenk line configuration was used for nanocrystal synthesis.

3.2 PbSe Nanocrystal Synthesis

The lead selenide nanocrystals were synthesized by a colloidal chemical process consisting of two separate liquid precursors as detailed in [23]. The initial selenium precursor was prepared by adding 0.315 g of selenium powder to a scintillation vial, which was then loaded into a glove box with a nitrogen atmosphere. Once in the glove box, 4 ml of trioctylphosphine was added to the vial. A micropipette was used to add 30 µL of diphenylphosphine, a catalyst for the growth procedure, to the mixture. The vial was then heated at 60 ^{o}C and stirred overnight.

The lead precursor was prepared immediately prior to the synthesis procedure. A 25 ml three-neck flask was loaded with 0.3 g of lead oxide powder, 1.05 ml of oleic acid, and 5.3 ml of octadecene. The three-neck flask was added to a Schlenk line as show in Figure 3.1.1 and placed under a nitrogen atmosphere. The flask was heated to 140 ^{o}C and stirred for an hour to ensure complete dissolution of the lead oxide. The above procedure, including all amounts, will be referred to as a "standard-yield synthesis." A double-yield synthesis would be the same procedure with doubled amounts.

Once the lead was completely dissolved, the selenium precursor was loaded into a 10 ml syringe, removed from the glove box, and then injected into the three-neck flask through a rubber cap on one of the necks. The mixture was allowed to react for 20 seconds before the flask was quenched in room-temperature water. This will be referred to as the reaction time. The quenching was continued until the solution reached 30 ^{o}C.

After the synthesis, the solution was purified by the following process. The solution was separated into four centrifugation tubes with approximately 5 ml of nanocrystal solution each.

The remaining space in each tube (approximately 45 ml) was filled with acetone and shaken until the solution was homogenous. The tubes were then loaded into a Labnet Hermle Z-300 and centrifuged at 6000 RPM for 5 minutes. This caused the nanocrystals to precipitate from the solution. This was done to remove any excess chemicals from the mixture. The excess acetone was discarded. The nanocrystals in each tube were dispersed using 5 ml of chloroform or hexane then filled with acetone again. This process was repeated four times.

3.3 PbSe Nanocrystal Characterization

The effective band gap of the nanocrystals can be determined from the absorbance spectrum by

$$E = \frac{hc}{\lambda} \qquad \text{(Equation 3.1)}$$

where E is the band gap energy, h is the Planck constant, c is the speed of light, and λ is the wavelength that corresponds to the edge of the absorbance spectrum. This calculation can be compared to the band gap of the bulk material to determine whether or not nanocrystals were produced. The effective band gap of a nanostructure is expected to be wider than that of bulk. This corresponds to a shorter wavelength of absorbed photons.

Absorbance spectra were obtained for these nanocrystals using a UV-Vis-NIR spectrophotometer. A baseline of pure chloroform was obtained and subsequently subtracted from all trials with nanocrystals. Four nanocrystal trials were performed, with increasing concentration of nanocrystals in a chloroform solution on each successive trial. The results are contained in Figure 3.3.1. The absorbance measurements for chloroform are saturated from 1600-1800 nm, so this range has been omitted from Figure 3.3.1. As the wavelength approaches

400 nm, the glass vial begins to block the transmission, leading to an increase in measured absorbance.

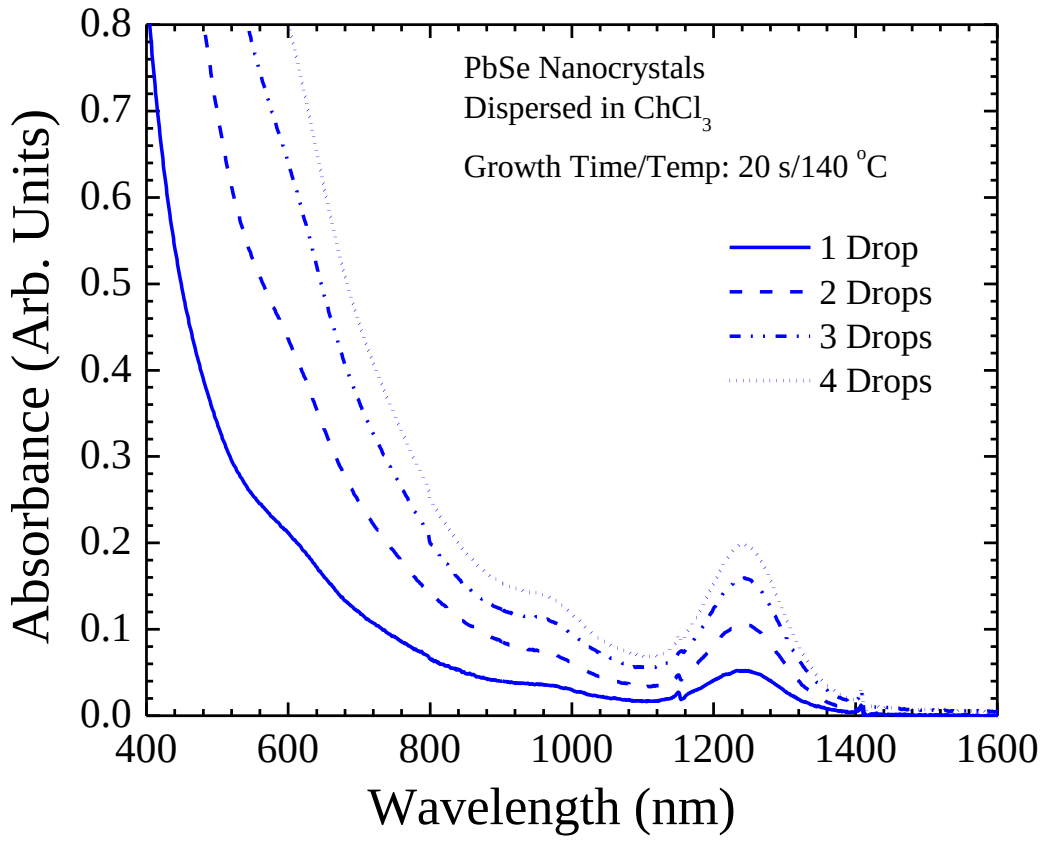

Figure 3.3.1. The absorbance spectrum for lead selenide nanocrystals dispersed in chloroform is shown. Nanocrystals were grown at 140 °C for 20 seconds.

Several points of interest can be seen in Figure 3.3.1. The peak located at 1240 nm corresponds to the first interband transition. The disturbances at 980 nm and approximately 600 nm correspond to transitions with higher energy. The visibility of these peaks suggests nanocrystals of high purity. As shown in Equation 3.1, the absorbance band edge can be used to calculate the band gap. Estimating this wavelength at $\lambda = 1400$ nm yields an effective band gap of 1.4×10^{-19} J, or 0.89 eV. This is of particular interest because the band gap of bulk lead

selenide is 0.27 eV. This is entirely due to the quantum confinement caused by the size of the nanocrystals. Transmission electron microscopy images and the energy-dispersive X-ray spectrum were obtained for these nanocrystals as seen in Figure 3.3.2 and Figure 3.3.3, respectively. It should be noted that the apparent presence of copper in the nanocrystals is due to the copper plate on which they were loaded, not any actual copper in the samples.

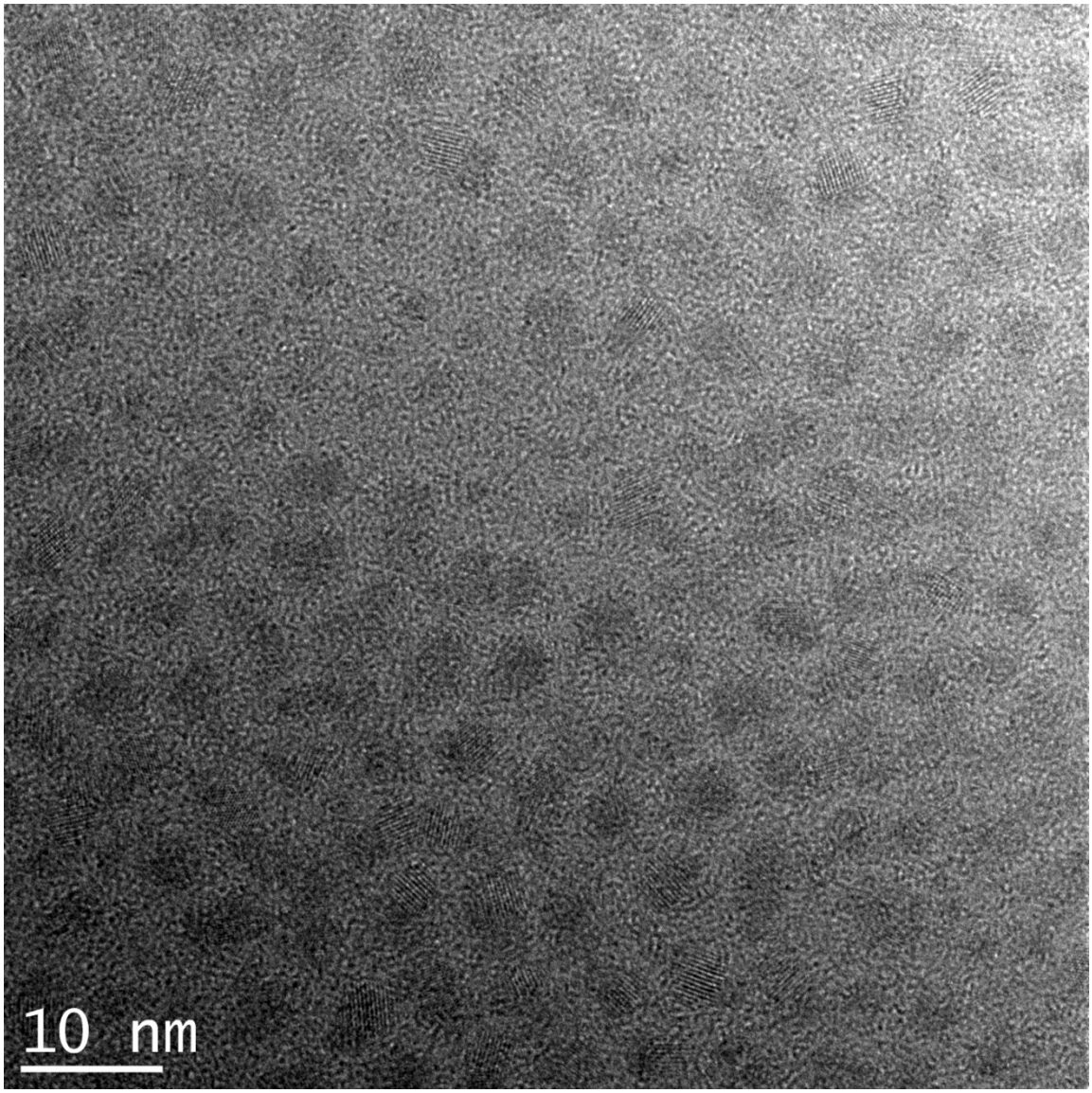

Figure 3.3.2. Transmission microscopy imaging was performed on the lead selenide nanocrystals.

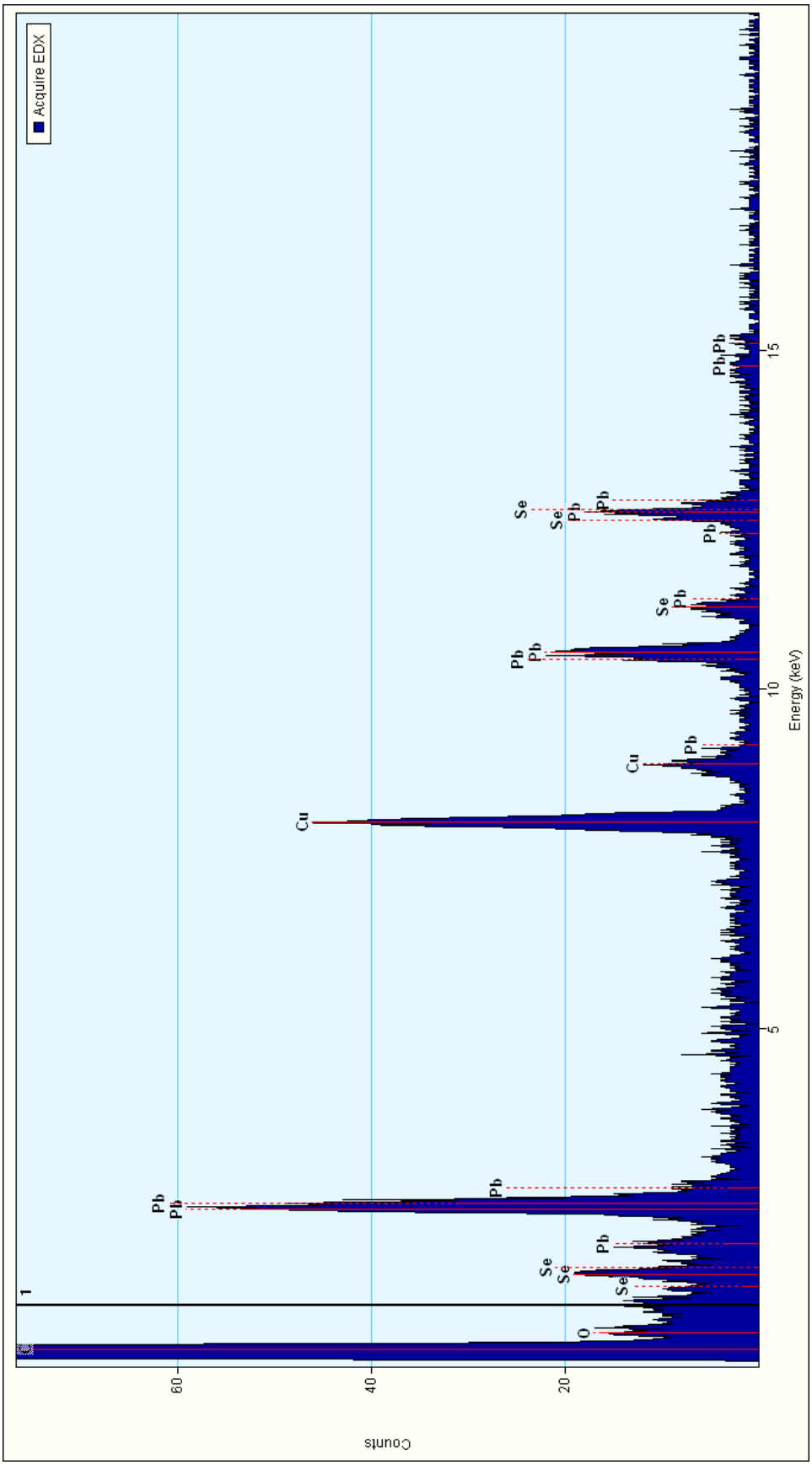

Figure 3.3.3. Energy-dispersive X-ray spectrum for lead selenide nanocrystals.

The photoluminescence spectrum was also obtained for these nanocrystals using a Bomem DA8 Fourier transform spectrometer. The nanocrystal samples were loaded into a cryostat and cooled to 77 K using liquid nitrogen to reduce thermal contributions. The photoluminescence spectrum is shown in Figure 3.3.4.

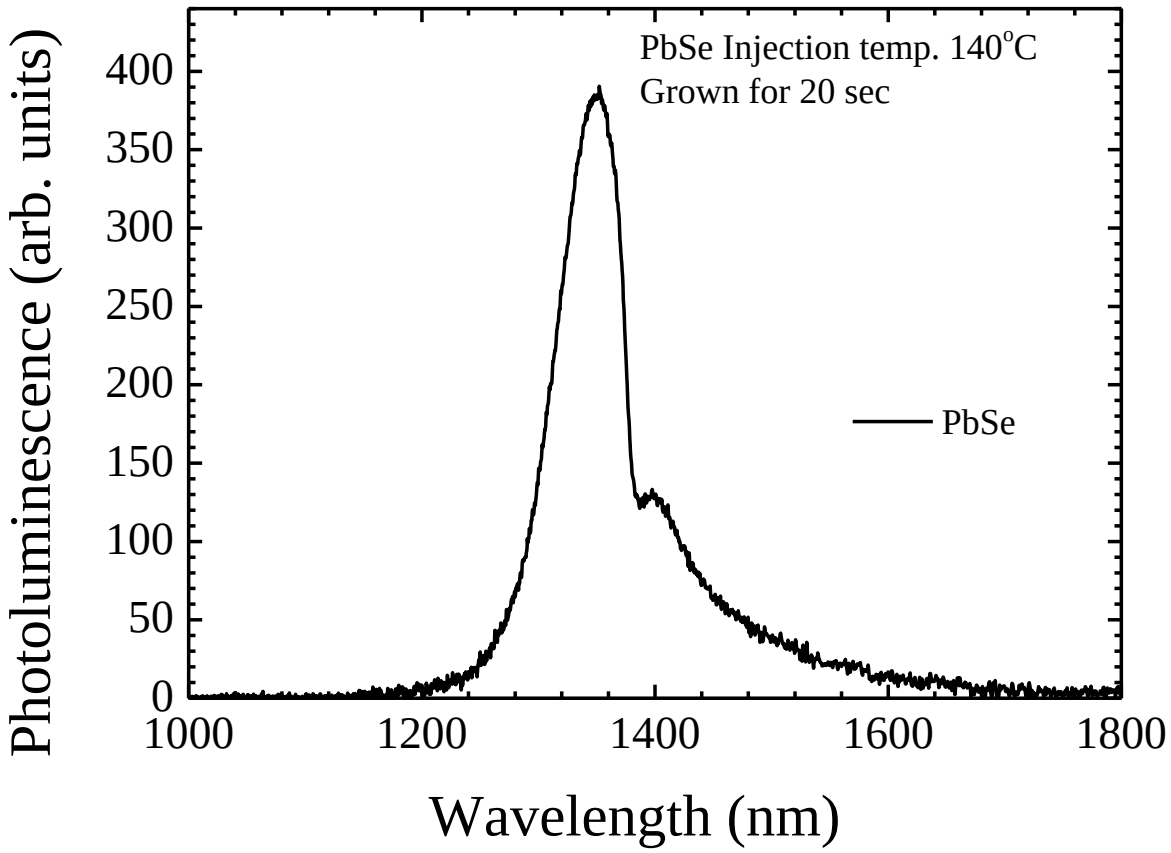

Figure 3.3.4. The photoluminescence spectrum was obtained for lead selenide nanocrystals grown at 140 °C for 20 seconds.

It is important to note that the peak position of the photoluminescence spectrum is located at approximately 1360 nm, while the absorbance peak was located at 1240 nm. This difference is due primarily to an effect known as the Stoke's shift. This happens when an excited electron recombines with a hole in the valence band while also emitting a phonon. The released phonon

removes energy from the emitted photon, resulting in an emission with lower energy than that of the photon responsible for exciting the electron. There is a smaller, secondary peak at 1400 nm, which is due to the existence of a second primary size of nanocrystal in the sample. The existence of this second size is due to factors such as the injection time during synthesis. The injection of the selenium precursor into the lead precursor is not an instantaneous event, thus some nanocrystals have longer reaction times than that of other nanocrystals. Ideally, the PL spectrum would look like a Dirac delta function. The full width at the half maximum is 60 nm.

3.4 PbSe Photodetector Fabrication

An interdigital contact structure was used for the photodetectors in this research. Photodetectors with channel widths of 20 and 50 μm were fabricated. A depiction of channel width is shown in Figure 3.4.1.

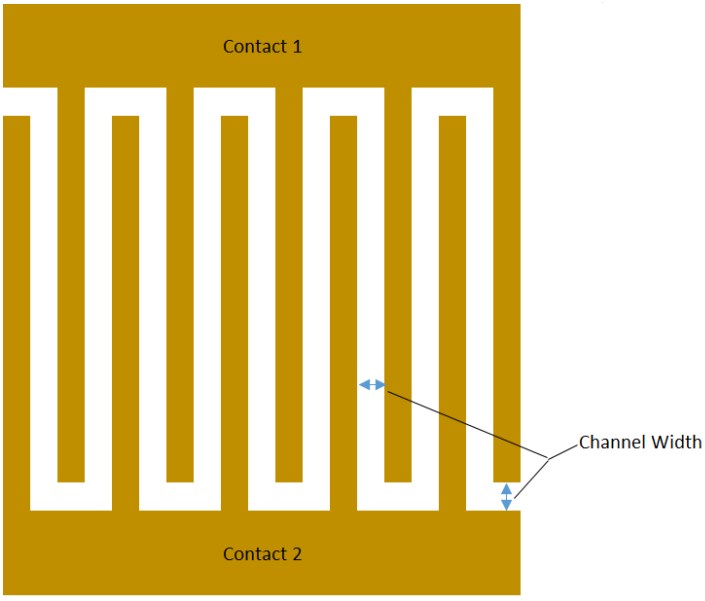

Figure 3.4.1. An interdigital photodetector contact structure was chosen for this research.

Spin coating was used to deposit a layer of positive photoresist on a glass slide. This photoresist was exposed to ultraviolet light with an interdigital mask pattern. The photoresist was developed using photoresist developer such that the contact area was free of photoresist. The glass was then loaded into an Angstrom Engineering Nexdep physical vapor deposition system. Gold was deposited on top of the glass and remaining photoresist layer. Acetone was used to dissolve the remaining photoresist and attached gold, leaving only the gold in the desired contact geometry. Figure 3.4.2 shows the completed contact structure.

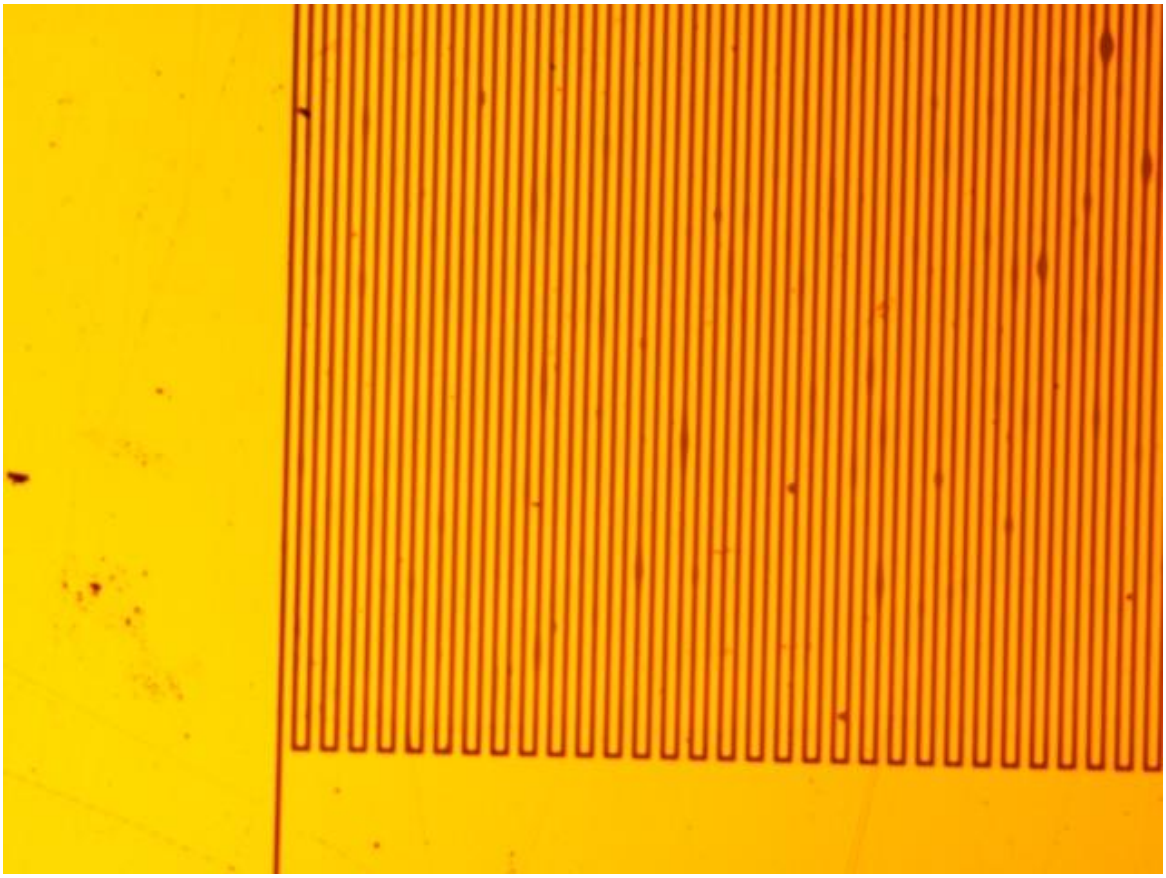

Figure 3.4.2. Gold contacts were deposited on a glass substrate in an interdigital pattern. Structures with 20 µm and 50 µm channels were fabricated.

Nanocrystals could not be added to the interdigitated structure immediately after synthesis due to the oleic acid ligands surrounding them. These ligands are long hydrocarbon chains and are very resistive. Thus, they would impair the sensing capabilities of the photodetector. To overcome this limitation, the long oleic acid ligands were exchanged for two shorter, more conductive, hydrocarbons: ethanedithiol and mercaptoacetic acid. The exchange for mercaptoacetic acid was performed by mixing the oleic acid capped nanocrystals in mercaptoacetic acid. The solution was then heated to 60 ^{o}C and stirred for 48 hours. After this, the same purification procedure that was used after synthesis was employed to clean the nanocrystals. Sonication was required in order to disperse the nanocrystals in chloroform. After purification, absorbance was measured with increasing concentration to verify the integrity of the nanocrystals. The absorbance spectrum can be seen in Figure 3.4.3.

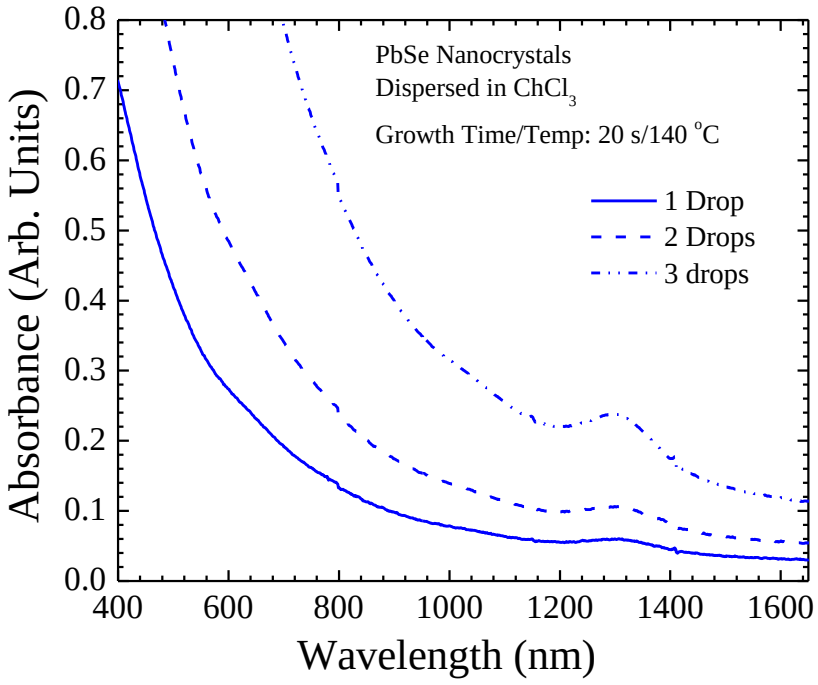

Figure 3.4.3. Absorbance spectra were obtained for three different concentrations of lead selenide nanocrystals capped with mercaptoacetic acid.

The peak position of the absorbance spectrum in Figure 3.4.3 is offset from the original shown in Figure 3.3.1 by about 60 nm. The exact reason for this is unknown, but this could be caused by mild aggregation of the nanocrystals or oxidation.

The next step in the fabrication of the detector was attaching the substrate to a mounting plate and wiring the contacts. Once the wiring was complete, the nanocrystals with mercaptoacetic acid ligands were dispersed in chloroform and deposited into the interdigital channel by drop casting. Current-voltage characterization was performed using a semiconductor characterization system as seen in Figure 3.4.4.

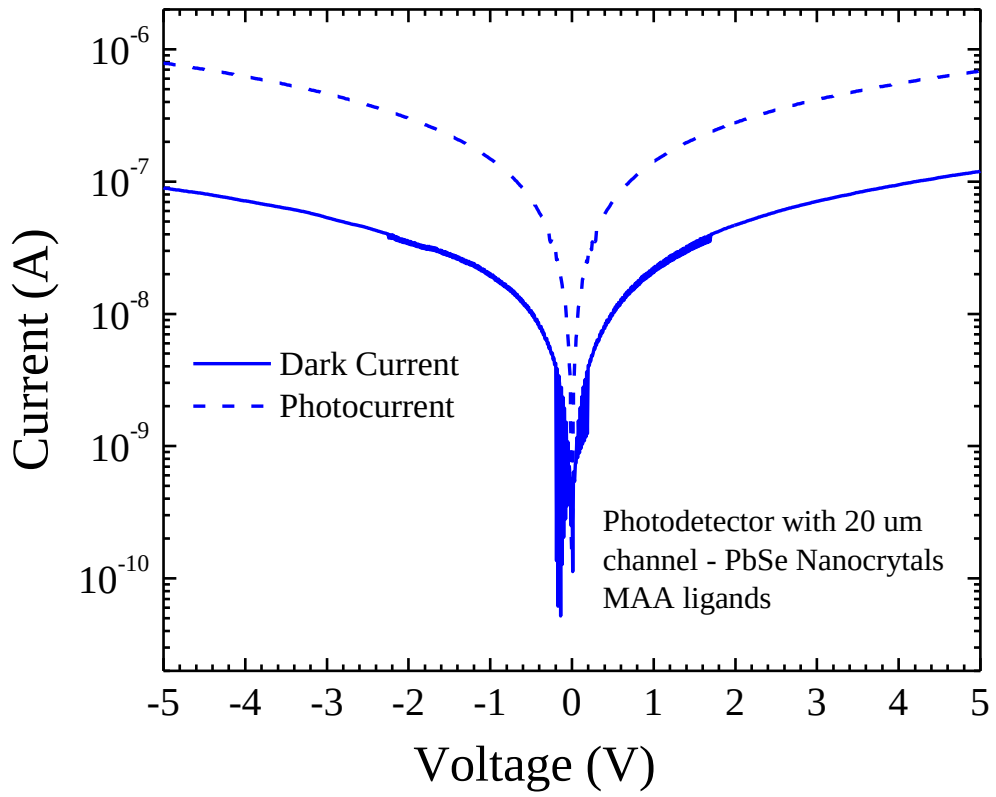

Figure 3.4.4. Lead selenide nanocrystals with mercaptoacetic acid ligands were added to an interdigital contact structure. Current-voltage characterization was performed.

The dark current was measured in complete darkness and the photocurrent was measured under 1 sun (100 mW/cm2) of irradiance. The magnitude of the current-voltage curve is shown in Figure 3.4.4. At ±5 V bias, there is approximately one order of magnitude of enhancement from the dark current to the photocurrent. This measurement was performed on a photodetector with a 20 μm channel. Using Equations 2.5 and 2.6, the responsivity and specific detectivity of this photodetector were calculated. They are shown in Figures 3.4.5 and 3.4.6, respectively.

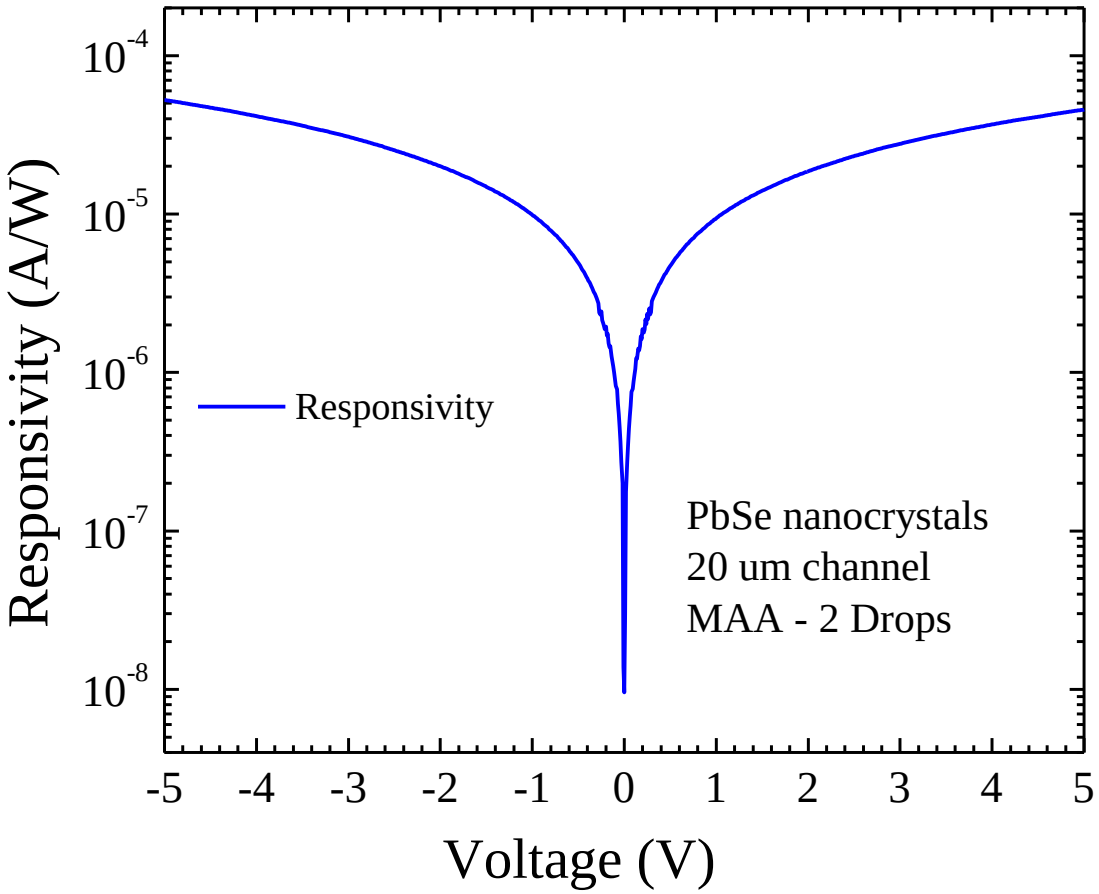

Figure 3.4.5. Responsivity of the photodetector was calculated from the current-voltage characteristics.

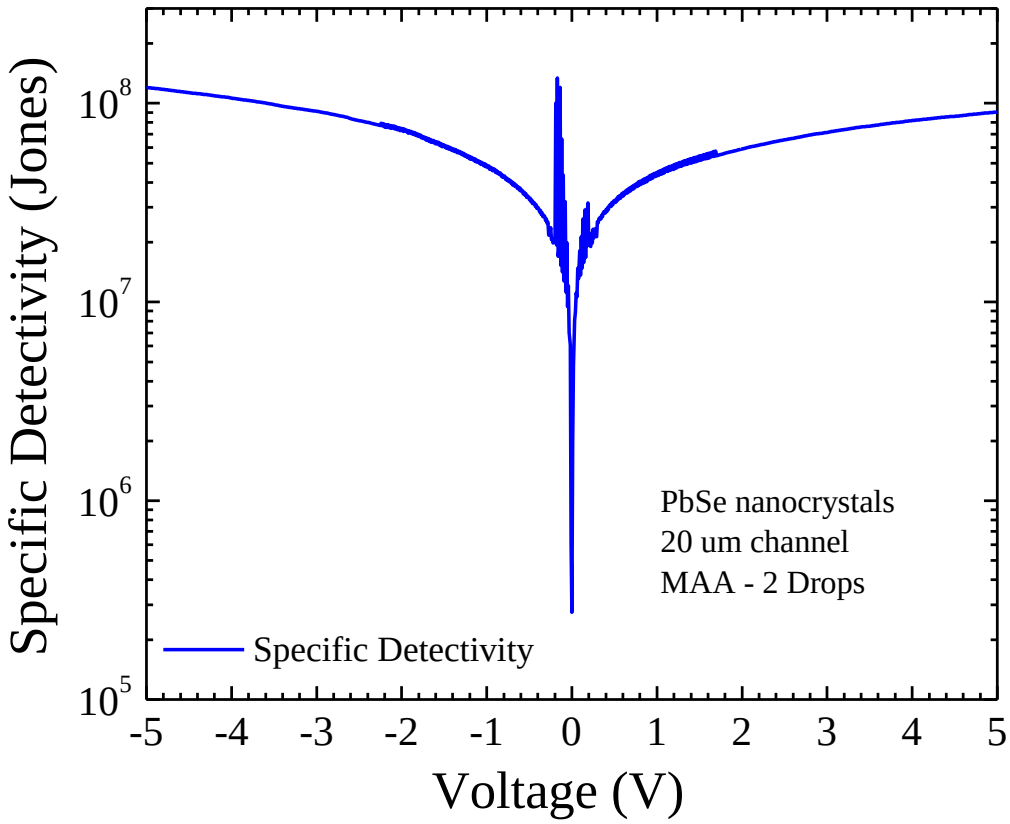

Figure 3.4.6. Specific detectivity was calculated using the responsivity and current-voltage characteristics.

The specific detectivity of this photodetector with a bias voltage of -5 V is 1.1×10^8 Jones, which is comparable to literature [10].

A second and third photodetector, one with a 50 μm channel and the other with a 10 μm channel, were fabricated. The method of contact deposition previously described was insufficient for creating a 10 μm device, as the liftoff procedure consistently left shorts in the device or removed the interdigital structure altogether. The 50 μm device showed very little enhancement in the dark current. This is unlikely to be due to a short, as the dark current was approximately 10^{-8} A. A more likely explanation is that the mercaptoacetic acid ligands were not

conductive enough to permit a channel width of that size. Because of this, a different ligand was chosen: ethanedithiol.

Ethanedithiol was reported by [24] to allow for more conductive thin films of nanocrystals to be deposited. The process detailed by Luther et al. required alternating sequences of dipping the sample in ethanedithiol and lead selenide nanocrystals. For this research, a MTI PTL-OV5P Dip Coater was used to control the rate at which the dipping occurred. Two separate beakers, one containing oleic acid capped lead selenide nanocrystals dispersed in chloroform and the other containing ethanedithiol, were placed in the dip coater. The 50 μm photodetector contacts were then lowered first into the nanocrystals and then into the ethanedithiol. The process was repeated several times to coat the detector with a uniform film of nanocrystals. As the nanocrystals were dipped into the ethanedithiol, the oleic acid ligands were removed and replaced. Three trials were performed to observe the effect of number of dips on conductivity and photoresponse. The current-voltage characteristics of these trials are shown in Figures 3.4.7, 3.4.8, and 3.4.9.

After five dips in nanocrystals and ethanedithiol, there was approximately half an order of magnitude of enhancement between the dark current and the photocurrent. The dipping process was repeated another five times, resulting in one order of magnitude enhancement of the photocurrent. The dark current and photocurrent at ±5 V were measured at 10^{-6} A and 10^{-5} A, respectively. After five more dips, there was no further substantial enhancement of the photocurrent. However, the dark current was increased by approximately half an order of magnitude. This was undesirable for a few reasons. By considering Equations 2.5 and 2.6, it is relatively simple to see that a large separation between the photocurrent and dark current is desirable to produce a detector with high specific detectivity.

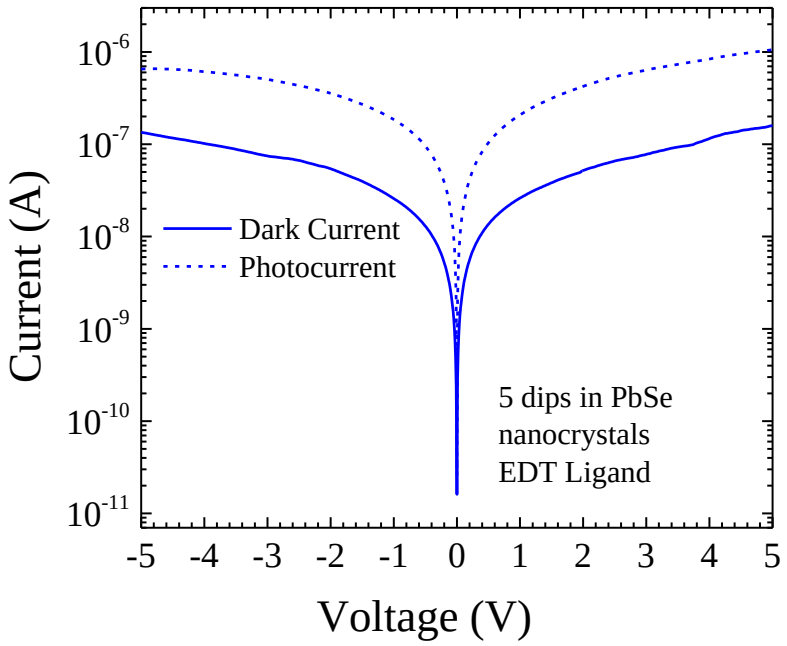

Figure 3.4.7. Current-voltage characterization was performed after five dips in ethanedithiol.

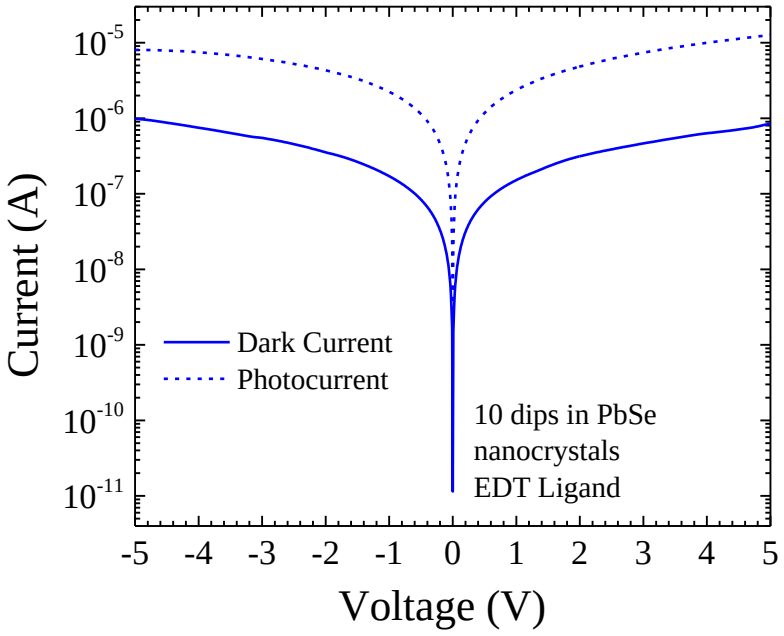

Figure 3.4.8. Current-voltage characterization was performed after 10 dips in ethanedithiol.

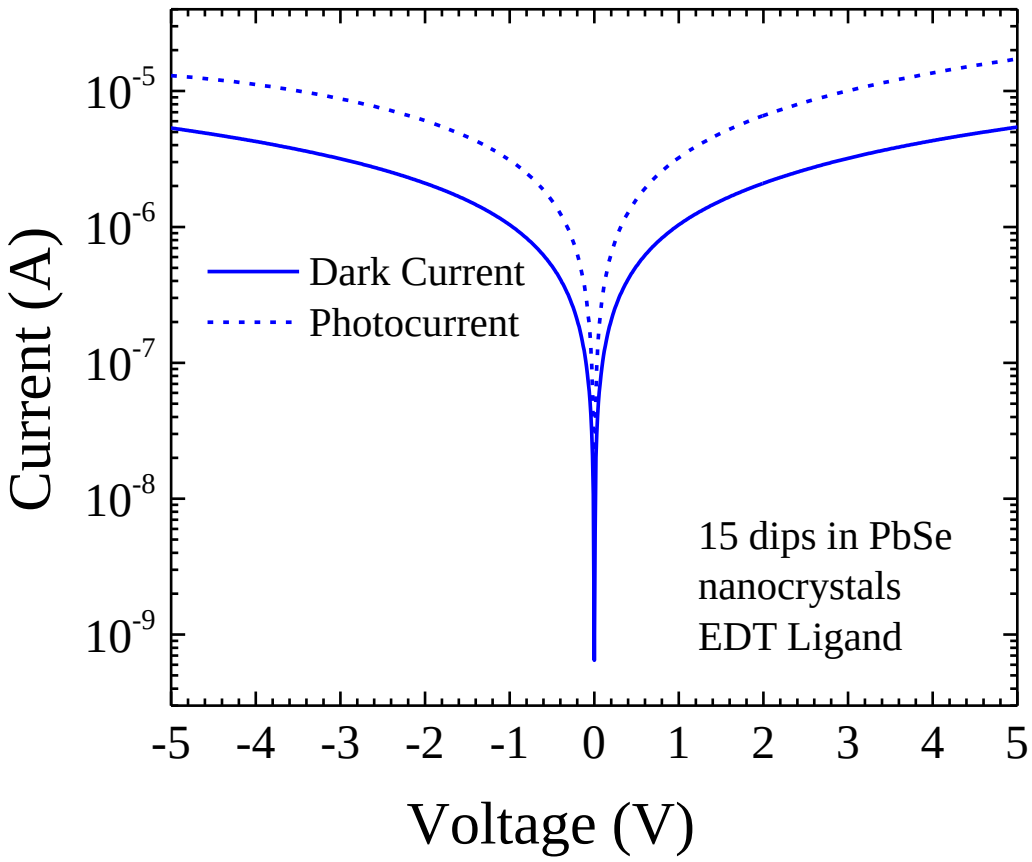

Figure 3.4.9. Current-voltage characterization was performed after 15 dips in ethanedithiol.

Because of the large difference in the photocurrent and dark current present in Figure 3.4.8, the 10-dip device was determined to have the highest specific detectivity. Furthermore, a high dark current means that more current passes through the device, even when there is no incident light. This in turn means that the device would dissipate more power than one with a low dark current. In addition to using more energy to operate, this could cause heating in the nanocrystals. Excess thermal energy could contribute to optical excitation of the electrons. Thermal excitation would result in increased conductivity, thus causing noise in the signal. This

would require a cooling mechanism to combat, thus removing one of the main advantages of using nanostructures.

A 20 µm device was also attempted with this method, but was far too conductive with the ethanedithiol ligands. After two dips in ethanedithiol, the dark current rose to 10^{-2} A with very little enhancement of the photocurrent. Attempts were made to reduce the concentration of nanocrystals and ethanedithiol to produce a 20 µm device but all attempts produced similar results. The responsivity and specific detectivity of the 50 µm device are shown in Figures 3.4.10 and 3.4.11, respectively. At 5 V bias, the 50 µm ethanedithiol device produces a specific

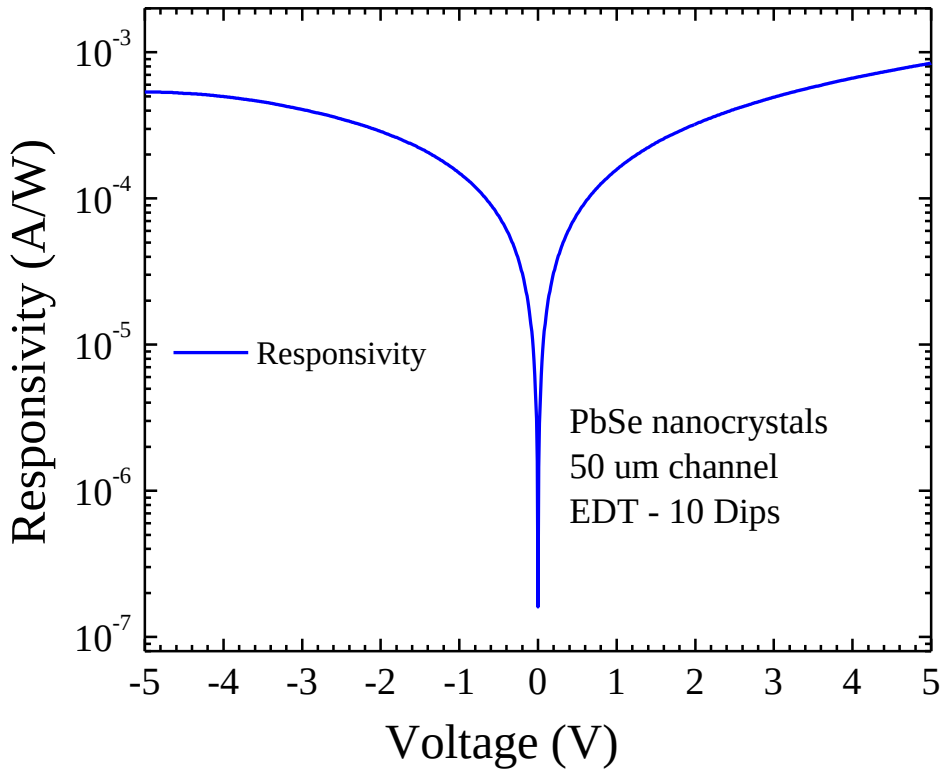

Figure 3.4.10. A photodetector with a 50 µm channel filled was dipped in ethanedithiol and lead selenide nanocrystals 10 times. The responsivity was calculated from the current-voltage characteristics in Figure 3.3.8.

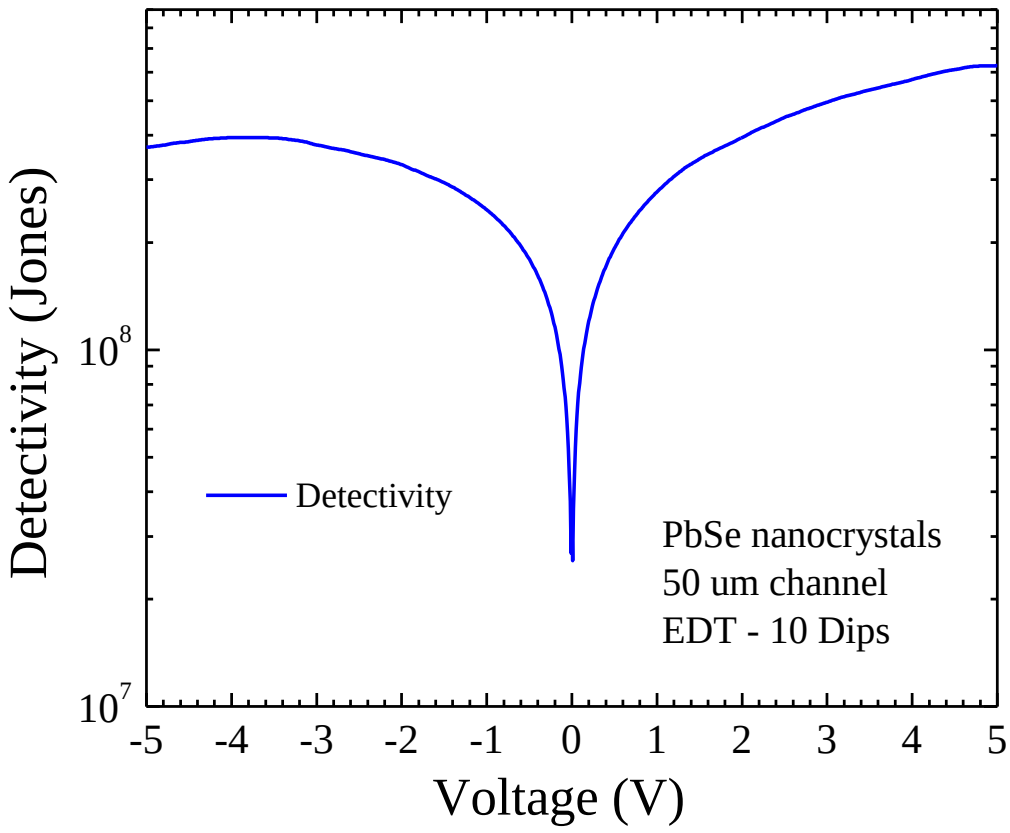

Figure 3.4.11. A photodetector with a 50 µm channel filled was dipped in ethanedithiol and lead selenide nanocrystals 10 times. The specific detectivity was calculated from responsivity in Figure 3.4.10 and the current-voltage characteristics in Figure 3.4.8.

detectivity that is approximately half an order of magnitude larger than that of the mercaptoacetic acid device, despite having a wider channel.

Spectral response measurements were performed using a Fourier transform spectrometer. Despite the poor current-voltage characteristics of the 50 µm channel detector with mercaptoacetic acid-capped nanocrystals, it was possible to obtain spectral response measurements for both the 20 µm and 50 µm devices. These measurements were plotted together for comparison in Figure 3.4.12.

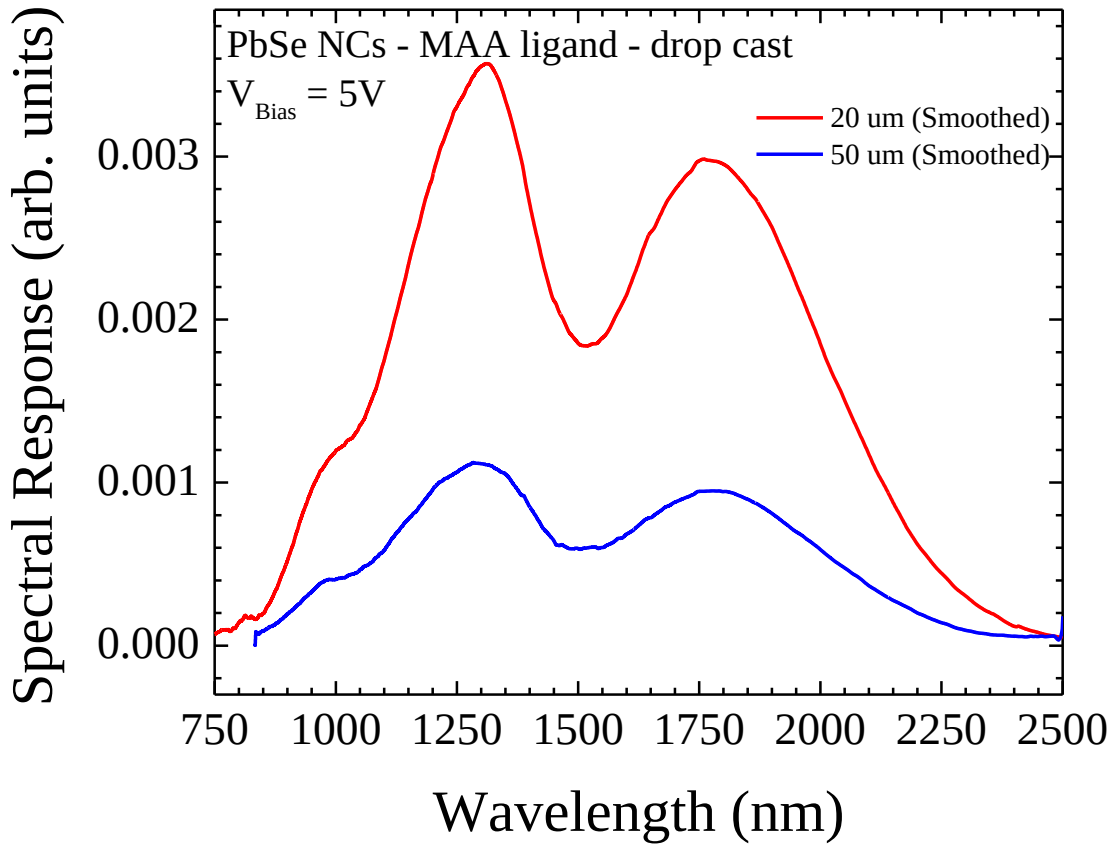

Figure 3.4.12. Spectral response was measured for 20 µm and 50 µm photodetectors with mercaptoacetic acid-capped nanocrystals.

Both spectra in Figure 3.4.12 were measured with a 5 V bias at room temperature. Each device showed an unexpected peak at approximately 1800 nm. This is believed to be caused by oxidation of the nanocrystals on the surface. Oxidation of lead selenide can result in shifts of the absorbance and photoluminescence of the nanocrystals [25]. As expected, the response of the 20 µm device was far stronger than the 50 µm device. A device with smaller features would likely be even more responsive, assuming that the dark current remains low. A new fabrication process such as reactive ion etching could potentially be used to fabricate detectors with smaller channel widths.

Spectral response was also performed for the 50 µm ethanedithiol device. Again, the response was shifted, presumably by oxidation effects, but to less of a degree than the devices with mercaptoacetic acid-capped nanocrystals. The spectrum for the ethanedithiol device is shown in Figure 3.4.13.

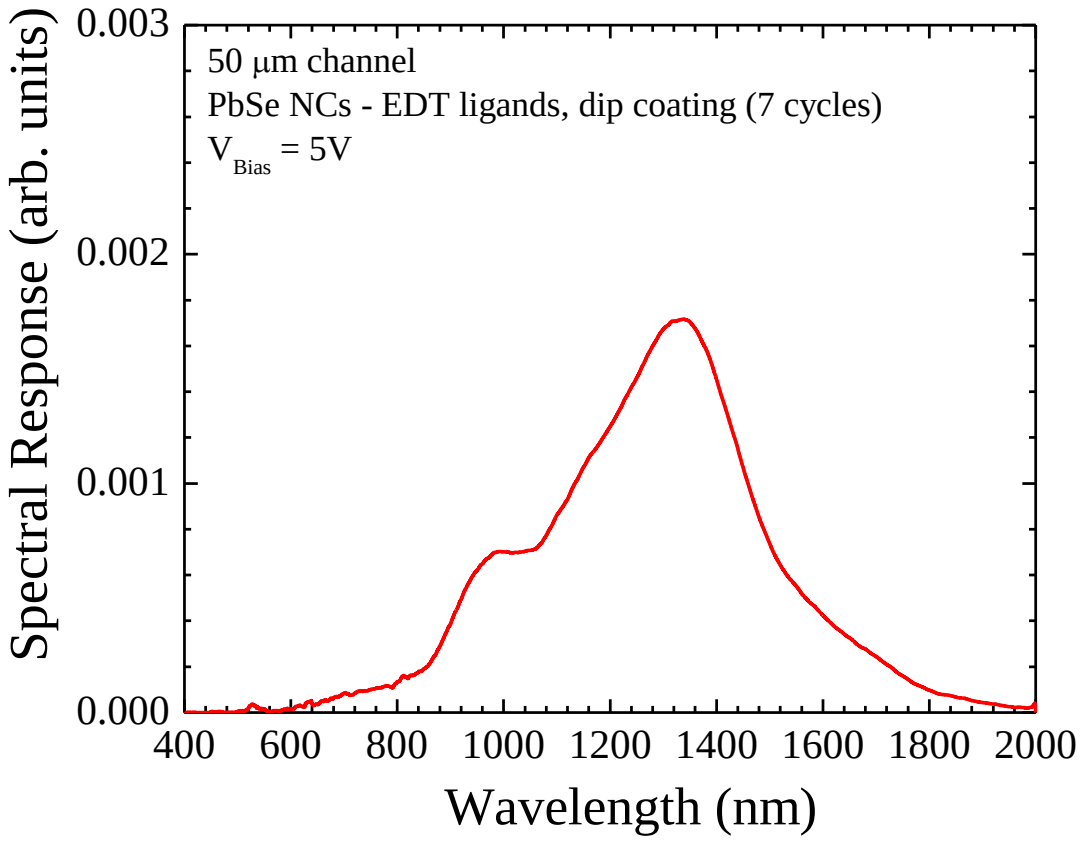

Figure 3.4.13. Spectral response was measured for the 50 µm photodetector with ethanedithiol-capped nanocrystals. Measurements were performed at room temperature with a 5 V bias.

The spectral response of the 50 µm detector with ethanedithiol-capped was stronger than that of the 50 µm device with mercaptoacetic acid-capped ligands, but weaker than that of the 20 µm device. Despite the difference in response strength, the ethanedithiol-capped nanocrystals

provided a narrower range. This may be due to differences in the time between fabrication and spectral response measurements. Due to equipment availability, more time passed between the fabrication of the mercaptoacetic acid-capped nanocrystals and the spectral response measurement than that of the ethanedithiol-capped nanocrystals. This would have resulted in more oxidation on the mercaptoacetic acid-capped nanocrystals than on those with ethanedithiol ligands.

3.5 PbSe/PbS Core/Shell Nanocrystal Synthesis

One possible solution to the problem of oxidation of the nanocrystals is creating a core/shell structure using a second type of material. Lead sulfide was chosen because it has a similar band gap to lead selenide (0.41 eV) [26]. Additionally, lead sulfide oxidizes at a slower rate than lead selenide [27]. Because the band gap of lead sulfide is not the same as that of lead selenide, the band structure becomes more complex. Transitions may occur in both the core and the shell, which will influence the electronic properties of the nanocrystals. By growing a shell around pre-formed lead selenide nanocrystals, the overall size of the structure will also be increased. These two effects, coupled with the fact that lead sulfide has a wider band gap than lead selenide, will result in nanocrystals that absorb larger wavelength, lower energy photons. The synthesis procedure used for the core/shell structure is outlined in [28]. The structure of the core/shell nanocrystal is shown in 3.5.1, along with a depiction of the energy band structure for this material. This diagram is a qualitative depiction of the structure and is not scaled to match the actual energy differences between lead selenide and lead sulfide. Additionally, the quantized energy levels are not shown due to the complexity of the levels in this type of structure.

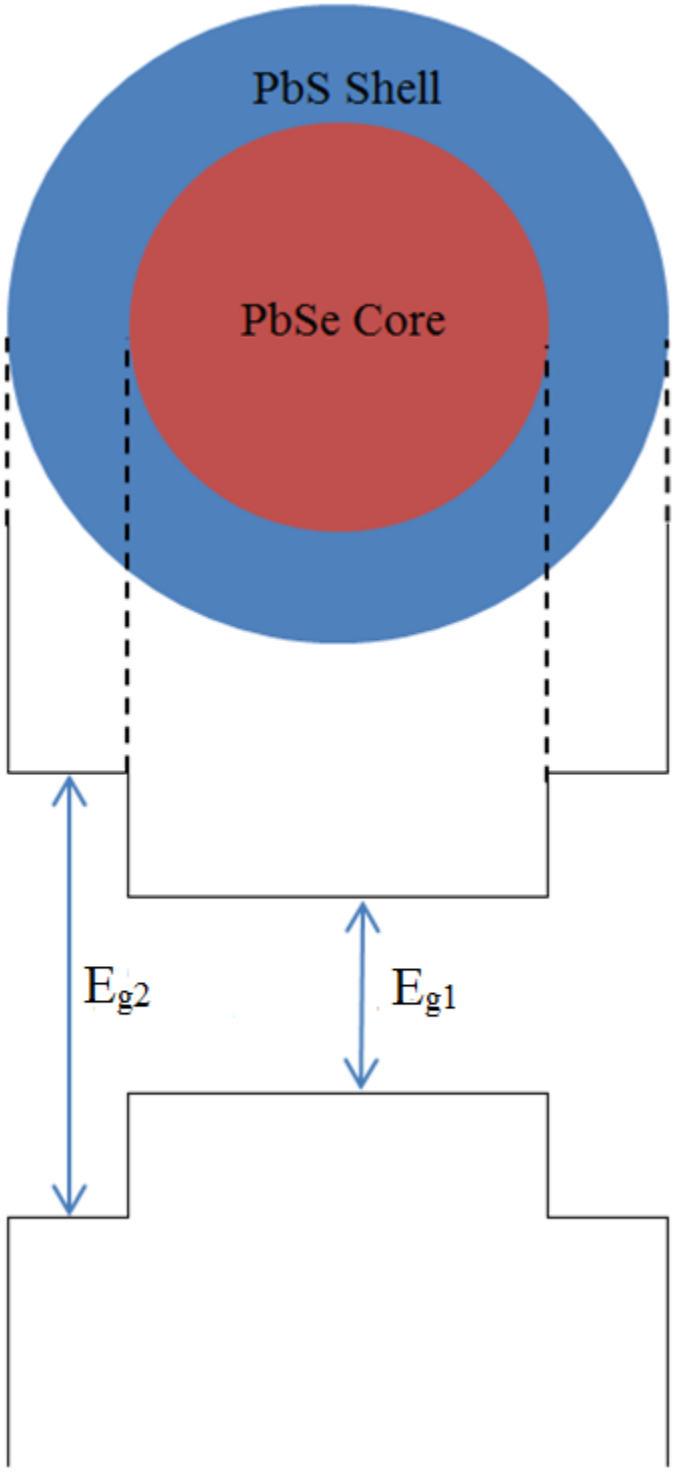

Figure 3.5.1. Lead selenide nanocrystals were synthesized. A lead sulfide shell was grown around the nanocrystals to create a core/shell structure. Lead sulfide has a larger band gap than that of lead selenide.

Lead selenide core nanocrystals were synthesized according to the procedure in Section 3.2. Lead sulfide shells were grown by a similar precursor injection method detailed in [28]. Lead selenide nanocrystals were dispersed in chloroform and mixed with 1.4 ml of trioctylphosphine. This mixture was heated at 60 ^{o}C and stirred to remove the chloroform. A second solution was created by combining 0.2 g of lead acetate, 2 ml of diphenyl ether, 1.5 ml of oleic acid, and 8 ml of trioctylphosphine in a three-neck flask under a nitrogen atmosphere on a Schlenk line. The three-neck flask was heated at 120 ^{o}C for an hour, and then cooled to 45 ^{o}C. The three-neck flask was moved to a glove box with a nitrogen atmosphere. This flask was maintained at 45 ^{o}C. A third solution was formed by dissolving 0.1 g of sulfur in 1 ml of trioctylphosphine. All three of these solutions were combined in the glove box at 45 ^{o}C. This will be referred to as the reagent solution.

A second three-neck flask is placed on the Schlenk line with 15 ml of diphenyl ether and heated to 180 ^{o}C. The reagent solution was loaded into two 10 ml syringes and removed from the glove box. The reagent solution was injected into the three-neck flask containing 15 ml of diphenyl ether. The injection resulted in a temperature drop from 180 ^{o}C to 120 ^{o}C. This temperature was maintained for a reaction time of 15 minutes. The three-neck flask was submerged in room temperature water to quench the reaction. The nanocrystals were split into six centrifugation tubes and purified in the same manner as the lead selenide core nanocrystals. Purification was performed five times.

This procedure required significant modification from [28] due to limitations in available equipment. The chemical yield was far lower than expected. Every synthesis resulted in an output to input ratio that was far less than one. Typical synthesis procedures involved adding approximately 150 mg of lead selenide cores, but would only produce 20-30 mg of core/shell

nanocrystals despite the addition of lead and sulfur reactants. The most likely reason for this is a stoichiometrically imbalanced reaction. The procedure listed in [28] failed to specify the quantity of lead selenide core nanocrystals required for the growth of lead sulfide shells.

Absorbance measurements were obtained for the lead selenide / lead sulfide core/shell nanocrystals. Two trials were performed with increasing concentration in chloroform. The results of these trials are contained in Figure 3.5.2.

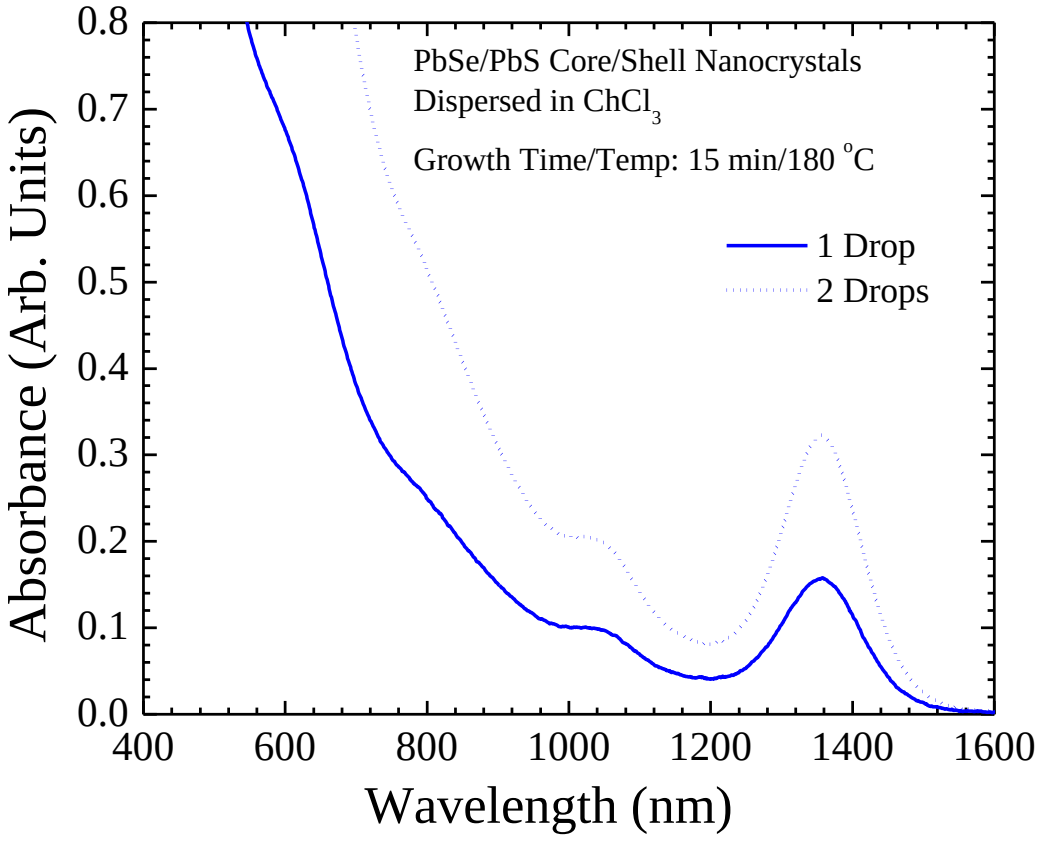

Figure 3.5.2. The absorbance spectra were obtained for lead selenide / lead sulfide core/shell nanocrystals.

The peak position of the core/shell nanocrystals is located at approximately 1360 nm. When comparing Figures 3.5.2 and 3.3.1, there is a red shift of approximately 120 nm. This is because the size of the nanocrystals is increased by the addition of the lead sulfide shell. The photoluminescence spectrum was obtained for the core/shell nanocrystals. The photoluminescence spectrum is shown in Figure 3.5.3.

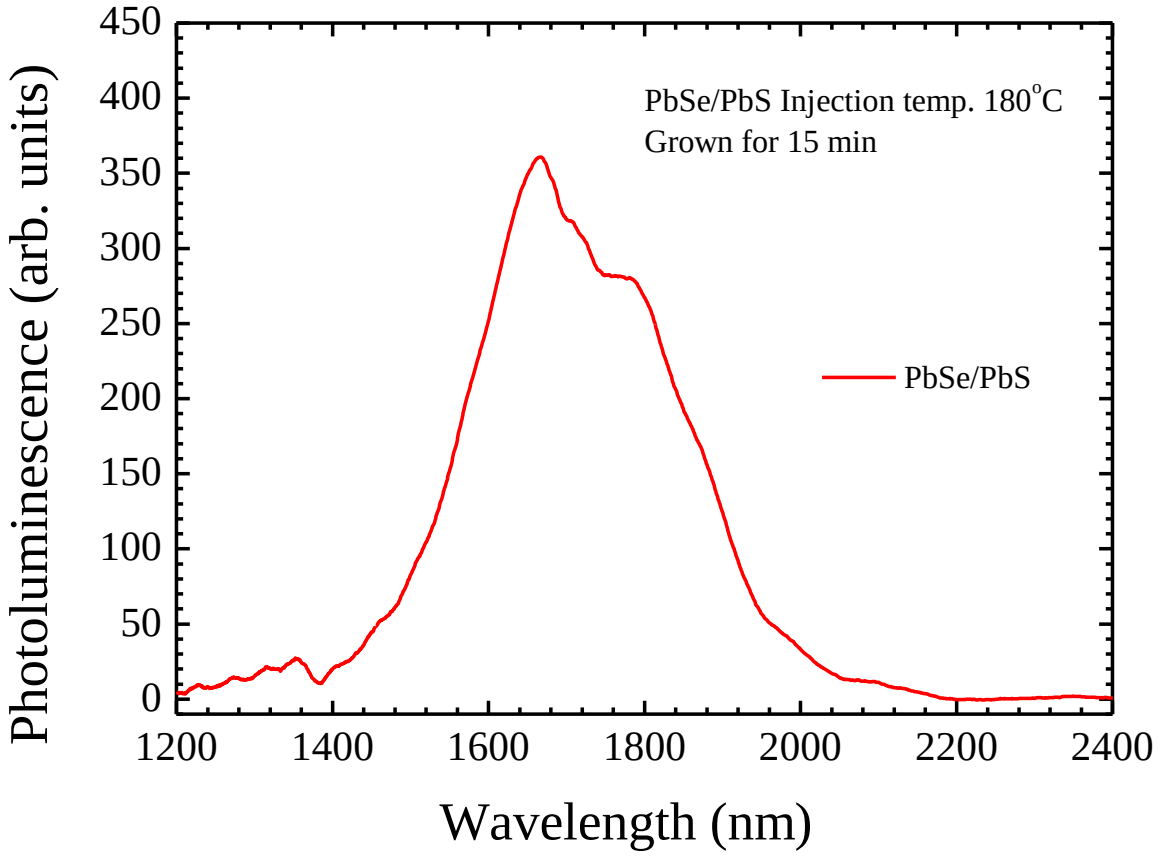

Figure 3.5.3. The photoluminescence spectra of lead selenide / lead sulfide core/shell nanocrystals was obtained. Measurements were performed at 77 K.

The large difference in peak positions between Figures 3.5.3 and 3.5.2 is due to phonon interactions. Since the emitted photons have less energy than the absorbed, this is a Stoke's shift

as opposed to an anti-Stoke's shift. Because the reaction time for the shell growth was much longer than that of the core, there was a much larger distribution of sizes in the nanocrystals. This is the primary cause of the wide photoluminescence peak in Figure 3.5.3. The full width at the half maximum for Figure 3.5.3 is 295 nm. Transmission electron microscopy was performed prior to synthesis of core/shell nanocrystals. Nanocrystals with diameters of approximately 5 nm were observed as shown in Figure 3.5.4.

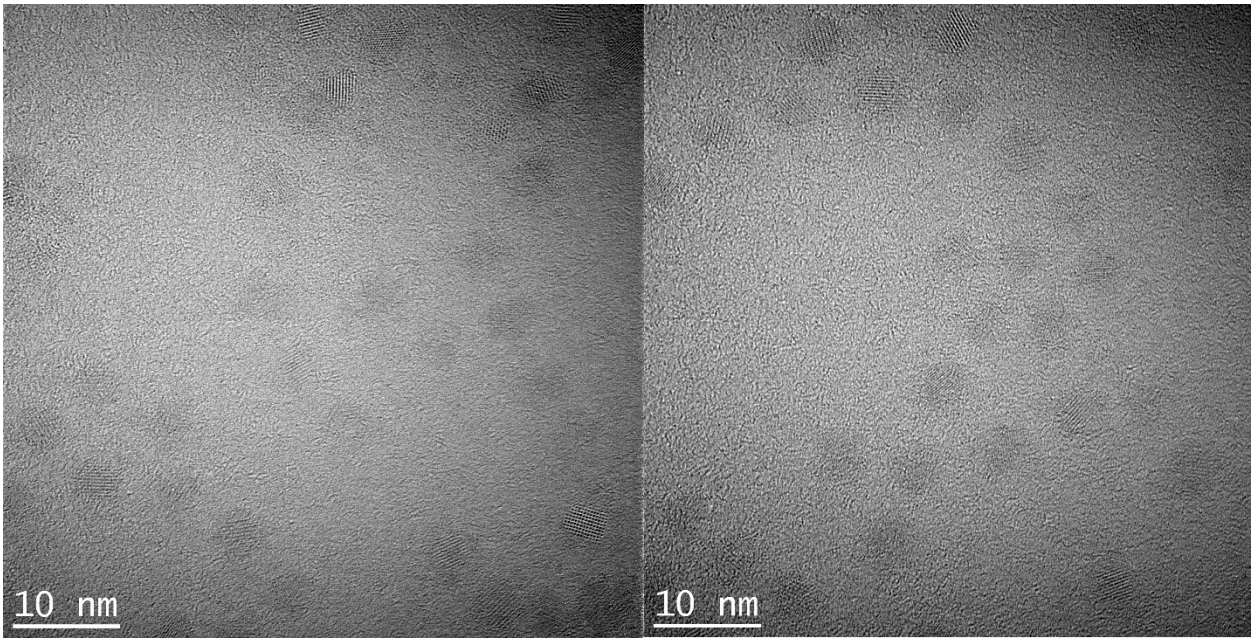

Figure 3.5.4. Lead selenide / lead sulfide core/shell nanocrystals were imaged with high resolution transmission electron microscopy.

Mercaptoacetic acid and ethanedithiol ligand exchange procedures were attempted with the core/shell nanocrystals but neither was successful. Both ligand exchange procedures resulted in excessive nanocrystal aggregation. Because of this, photodetectors could not be fabricated from this material. This could be a result of using lead selenide core nanocrystals that were synthesized according to a different process than described in [28]. A large amount of diphenyl

ether was used as the solution base as opposed to the octadecene used in the core synthesis. In addition, lead acetate was used as the lead precursor instead of lead oxide. The interactions of these materials could have prevented the ligand exchange from performing as expected.

Chapter 4: Summary and Future Work

4.1 Summary

Lead selenide nanocrystals were chosen for use in creating an infrared photodetector. Nanocrystals were synthesized via a colloidal process with lead and selenium precursor solutions according to the process in [23]. Absorbance, photoluminescence, and energy-dispersive X-ray analysis were performed on the synthesized lead selenide nanocrystals. The effective band gap of the grown material was determined to be 0.83 eV as opposed to the band gap of the bulk material (0.27 eV).

Oleic acid ligands were replaced with mercaptoacetic acid and ethanedithiol ligands due to their shorter, more conductive nature. After ligand exchange, mercaptoacetic acid-capped and ethanedithiol-capped nanocrystals were deposited on interdigital gold contacts by drop casting and dip coating, respectively. Photodetectors with channel widths of 20 and 50 μm were fabricated from nanocrystals with each ligand. Current-voltage characterization was performed on all devices, but only the 20 μm device with mercaptoacetic acid-capped nanocrystals and the 50 μm device with ethanedithiol-capped nanocrystals produced functional photodetectors. It was determined that the 50 μm mercaptoacetic acid device lacked the required conductivity to function properly. In contrast, the 20 μm ethanedithiol device was too conductive and produced a very high dark current. Responsivity and specific detectivity were calculated for both devices. Each produced a specific detectivity on the order of 10^8 Jones, though the device with ethanedithiol-capped nanocrystals was determined to have slightly higher specific detectivity and responsivity.

Spectral response was measured for both devices. In each case, the detectors showed an unexpected secondary peak. Oxidation of the nanocrystals was believed to be the cause of this

behavior. Core/shell structured nanocrystals were chosen as a potential solution to this problem. Lead sulfide was selected for the shell material due to its similar band gap and slower rate of oxidation [27].

A secondary growth procedure in which a layer of lead sulfide was grown on top of an already existing lead selenide core was chosen. The synthesis procedure was modified moderately from the process described in [28] due to equipment restraints. Lead selenide cores from the initial nanocrystal synthesis were used in this process. Due to uncertainties in the shell growth procedure, large chemical yields were not obtained. Absorbance and photoluminescence measurements spectra were obtained. The shell growth was observed to shift the peak positions of the core nanocrystals to larger wavelengths. This was determined to be a result of the increased size of the nanocrystals, which resulted in a narrower effective band gap. The ligand exchange processes used for the core nanocrystals resulted in excessive nanocrystal aggregation when used with the core/shell nanocrystals for unknown reasons.

4.2 Future Work

The first step in continuation of this work is finding a reliable, high yield process for growth of lead selenide / lead sulfide core/shell nanocrystals. Furthermore, a suitable ligand exchange procedure must be established for the core/shell nanocrystals. Alternative ligand choices may require consideration, as well as intermediate ligand stripping procedures in which the ligands are not simultaneously removed and replaced.

Additional forms of nanocrystals should also be investigated, including the alloyed core/shell structures mentioned in [28]. Alternative narrow band gap materials, such as indium

phosphide, indium arsenide, indium antimonide, and lead telluride should also be considered for room temperature photodetectors [29], [30].

More reliable deposition and liftoff procedures are required to fabricate interdigital contact structures with smaller features. Instead of wet chemical development, reactive ion etching could be used to produce devices with 5 or 10 μm feature sizes [31]. Channel widths of these sizes may require much less concentrated nanocrystal solutions when ethanedithiol ligands are used.

References

[1] M. J. Potasek, *High-Bandwidth Optical Networks and Communication*. Elsevier Inc., 2001, pp. 459-543

[2] J. Michel, J. Liu, and L. C. Kimerling, "High-performance Ge-on-Si photodetectors," *Nat. Photonics*, vol. 4, no. 8, pp. 527–534, 2010.

[3] E. Monroy, E. Muñoz, F. J. Sánchez, F. Calle, E. Calleja, B. Beaumont, P. Gibart, J. a Muñoz, and F. Cussó, "High-performance GaN p-n junction photodetectors for solar ultraviolet applications," *Semicond. Sci. Technol.*, vol. 13, no. 9, pp. 1042–1046, 1999.

[4] Y. Jin, J. Wang, B. Sun, J. C. Blakesley, and N. C. Greenham, "Solution-processed ultraviolet photodetectors based on colloidal ZnO nanoparticles," *Nano Lett.*, vol. 8, no. 6, pp. 1649–1653, 2008.

[5] C. Dorrer, "High-speed measurements for optical telecommunication systems," *IEEE J. Sel. Top. Quantum Electron.*, vol. 12, no. 4, pp. 843–858, 2006.

[6] S. McDonald, G. Konstantatos, and S. Zhang, "Solution-processed PbS quantum dot infrared photodetectors and photovoltaics," *Nat. Mater.*, vol. 4, no. 2, pp. 138–42, 2005.

[7] K. Northon, "From Mountains to Moons: Multiple Discoveries from NASA's New Horizons Pluto Mission," 2015. [Online]. Available: http://www.nasa.gov/press-release/from-mountains-to-moons-multiple-discoveries-from-nasa-s-new-horizons-pluto-mission. [Accessed: 01-Jan-2016].

[8] M. Oehme, K. Kostecki, K. Ye, S. Bechler, K. Ulbricht, M. Schmid, M. Kaschel, M. Gollhofer, R. Körner, W. Zhang, E. Kasper, and J. Schulze, "GeSn-on-Si normal incidence photodetectors with bandwidths more than 40 GHz.," *Opt. Express*, vol. 22, no. 1, pp. 839–46, 2014.

[9] A. Rogalski, *Infrared Detectors*, vol. 43, no. 3–5. Gordon and Breach Science Publishers, 2000, pp. 87-95

[10] S. F. Tang, S. Y. Lin, and S. C. Lee, "Near-room-temperature operation of an InAs/GaAs quantum-dot infrared photodetector," *Appl. Phys. Lett.*, vol. 78, no. 17, pp. 2428–2430, 2001.

[11] A. M. Jawaid, D. J. Asunskis, and P. T. Snee, "Shape-controlled colloidal synthesis of rock-salt lead selenide nanocrystals," *ACS Nano*, vol. 5, no. 8, pp. 6465–6471, 2011.

[12] M. A. Omar, *Elementary solid state physics: principles and applications*. Addison Wesley Publishing Company, 1993, pp. 158-196

[13] O. Manasreh, *Introduction to Nanomaterials and Devices*. John Wiley and Sons, 2011, pp. 46-64

[14] S. I. Pokutnii, "Exciton binding energy in semiconductor quantum dots," *Semiconductors*, vol. 44, no. 4, pp. 488–493, 2010.

[15] W. J. Lorenz, G. Staikov, W. Schindler, and W. Wiesbeck, "The role of low-dimensional systems in electrochemical phase formation and dissolution processes," *J. Electrochem. Soc.*, vol. 149, no. 12, pp. K47--K59, 2002.

[16] C. B. Murray, S. Sun, W. Gaschler, H. Doyle, T. a. Betley, and C. R. Kagan, "Colloidal synthesis of nanocrystals and nanocrystal superlattices," *IBM J. Res. Dev.*, vol. 45, no. 1, pp. 47–56, 2001.

[17] P. Martyniuk and A. Rogalski, "Quantum-dot infrared photodetectors: Status and outlook," *Prog. Quantum Electron.*, vol. 32, no. 3–4, pp. 89–120, 2008.

[18] S. Baskoutas and A. F. Terzis, "Size-dependent band gap of colloidal quantum dots," *J. Appl. Phys.*, vol. 99, no. 1, 2006.

[19] M. Henini, "Semiconductors: Data Handbook," *Microelectronics J.*, vol. 35, no. 8, p. 685, 2004.

[20] I. H. J. Arellano, J. Mangadlao, I. B. Ramiro, and K. F. Suazo, "3-Component Low Temperature Solvothermal Synthesis of Colloidal Cadmium Sulfide Quantum Dots," *Mater. Lett.*, vol. 64, no. 6, pp. 785–788, 2010.

[21] D. Cui, J. Xu, S. Y. Xu, G. Paradee, B. A. Lewis, and M. D. Gerhold, "Infrared photodiode based on colloidal PbSe nanocrystal quantum dots," *IEEE Trans. Nanotechnol.*, vol. 5, no. 4, pp. 362–367, 2006.

[22] J. M. Pietryga, D. J. Werder, D. J. Williams, J. L. Casson, R. D. Schaller, V. I. Klimov, and J. A. Hollingsworth, "Utilizing the lability of lead selenide to produce heterostructured nanocrystals with bright, stable infrared emission," *J. Am. Chem. Soc.*, vol. 130, no. 14, pp. 4879–4885, 2008.

[23] A. Nusir, S. Member, J. Aguilar, J. Hill, H. Morris, M. O. Manasreh, and S. Member, "Uncooled Infrared Photodetector Utilizing PbSe Nanocrystals," *IEEE Trans. Nanotechnol.*, vol. 15, no. 1, pp. 109–112, 2016.

[24] J. M. Luther, M. C. B. Matt Law, Qing Song, Craig L. Perkins, and A. J. N. Nozik, and *, "Structural, optical, and electrical properties of self assembled films of PbSe nanocrystals treated with 1,2 ethanedithiol," *ACS Nano*, vol. 2, no. 2, pp. 271–280, 2008.

[25] J. S. Steckel, S. Coe-Sullivan, V. Bulović, and M. G. Bawendi, "1.3 μm to 1.55 μm Tunable Electroluminescence from PbSe Quantum Dots Embedded within an Organic Device," *Adv. Mater.*, vol. 15, no. 21, pp. 1862–1866, 2003.

[26] M. T. Nenadovic, M. I. Comor, V. Vasic, and O. I. Micic, "Transient bleaching of small lead sulfide colloids: influence of surface properties," *J. Phys. Chem.*, vol. 94, no. 16, pp. 6390–6396, 1990.

[27] M. H. Zarghami, Y. Liu, M. Gibbs, E. Gebremichael, C. Webster, and M. Law, "P-type PbSe and PbS quantum dot solids prepared with short-chain acids and diacids," *ACS Nano*, vol. 4, no. 4, pp. 2475–2485, 2010.

[28] M. Brumer, A. Kigel, L. Amirav, A. Sashchiuk, O. Solomesch, N. Tessler, and E. Lifshitz, "PbSe/PbS and PbSe/PbSexS1-x core/shell nanocrystals," *Adv. Funct. Mater.*, vol. 15, no. 7, pp. 1111–1116, 2005.

[29] S. Massidda, A. Continenza, A. J. Freeman, T. M. De Pascale, F. Meloni, and M. Serra, "Structural and electronic properties of narrow-band-gap semiconductors: InP, InAs, and InSb," *Phys. Rev. B*, vol. 41, no. 17, pp. 12079–12085, 1990.

[30] S. Ahmad, K. Hoang, and S. D. Mahanti, "Ab initio study of deep defect states in narrow band-gap semiconductors: Group III impurities in PbTe," *Phys. Rev. Lett.*, vol. 96, no. 5, pp. 1–4, 2006.

[31] Y. S. Zhen, M. S. Eng, and F. T. Aldridge, "High Speed Anisotropic Reactive Ion Etching of Gold Films," vol. 142, no. 5, pp. 127–129, 1995.

Appendix A: Description of Research for Popular Publication

Infrared photodetection is vitally important for many applications, such as telecommunications, space exploration, and imaging. Unfortunately, infrared detection systems often require complicated cooling systems to operate effectively, making them more costly. This work focuses on the creation of infrared detectors that function at room temperature by using novel materials. The materials in question are chemically grown lead selenide nanocrystals. These nanocrystals exhibit unusual properties not found in bulk lead selenide structures. Such properties are useful in the creation of high detectivity infrared detectors that function at all temperatures. Infrared imaging has many applications in everyday life. Firefighters use infrared sensors to locate people in burning buildings. Machinery operators can use infrared cameras to troubleshoot overheating equipment. Infrared photography allows for unique camera effects that are not otherwise possible. Night vision cameras rely on infrared light to produce images in complete darkness.

The band gap of a material is very important for describing why these materials are different from things that are seen in the naturally occurring world. The band gap is the amount of energy that is required to excite an electron to a new state. Stairs can be used as an analogy. In order to go up to the next floor, a person must have use energy. The amount of energy needed to get from the first floor to the second floor is analogous to the band gap in a semiconductor material. Just as a person changes "height levels" by using energy, the electrons change energy levels. One of the most commonly investigated properties of quantum structures is referred to as band gap tunability. This phenomenon occurs when the size of the material is constrained to very small sizes in at least one dimension. For lead selenide, the size must be reduced to approximately 50 nm (about 2000 times smaller than the width of a piece of paper) to see these

effects manifest. The nanocrystals in this research are constrained in three dimensions, resulting in further amplification of quantum effects. Because the size of these nanocrystals is on the order of 5-10 nm, the band gap is shifted from the bulk material by a larger margin. As the nanocrystals become larger, the band gap approaches that of the bulk material.

The quantum effects that arise due to restriction in the size of the structures are referred to as quantum confinement. These effects allow devices to be fabricated for highly specific applications. Because their band gap can be changed by alterations in the growth method, these nanocrystals can be very useful for designing devices that operate in regions not normally allowed by devices fabricated from bulk material.

The quantum structures described in this research were synthesized via a colloidal chemical reaction in which two precursor materials were combined. These precursors were allowed to react at a specific temperature for a limited time. At the end of this reaction time, the precursors were rapidly cooled to prevent further reaction. The precipitated nanocrystals were purified with centrifugation. After exchanging the initial ligands for shorter, more conductive ligands, the nanocrystals were deposited onto an interdigital contact structure for use as a photodetector.

Appendix B: Executive Summary of Newly Created Intellectual Property

Potential intellectual property includes:

- A synthesis method for producing lead selenide nanocrystals
- Fabrication process for producing an infrared photodetector that operates at room temperature

Appendix C: Potential Patent and Commercialization Aspects of Listed Intellecutal Property Items

C.1 Patentability of Intellectual Property

1. The synthesis procedure in this work was modified to fit the available equipment in Dr. Manasreh's lab at the University of Arkansas, Fayetteville. Because it is a new procedure for synthesis, this item could be patented.
2. The fabrication process used to create the photodetector contact structure, along with the deposition process of the nanocrystals, is a patentable process.

C.2 Commercialization Prospects

None of the previously listed intellectual property items are novel, and all should be apparent to an individual that is skilled in the art. As a result, these intellectual property items are not viable commercialization prospects.

C.3 Possible Prior Disclosure of Intellectual Property Items

All intellectual property contained in this work has been published. As a result, this work is considered to be in the public domain. No patent or commercialization aspects are available for the listed intellectual property items.

Appendix D: Broader Impact of Research

D.1 Applicability of Research Methods to Other Problems

Quantum structures are very useful for many optoelectronics applications. In addition to photodetection, they can be used for photovoltaics, light emitting diodes, and even have some applications in medical technology. Lead selenide in particular can also be used as a thermoelectric material. Similar methods could be utilized for other narrow band gap materials such as cadmium selenide, lead telluride, cadmium telluride, etc.

The synthesis procedure utilized in this research could also be easily adapted for colloidal nanocrystals of any material, assuming non-elemental structures such as pure gold nanoparticles. Different organic ligands could be used to provide varying levels of surface passivation, thus resulting in nanocrystals of larger or smaller diameters than those described in this work.

D.2 Impact of Research Results on U.S. and Global Society

Compared to expensive, high-purity semiconductor crystals, nanocrystals are very cheap to synthesize in an industrial environment. This technology could reduce the cost of production for electronic devices while also improving their capabilities. This would result in faster and more capable electronics, thus improving the quality of information transfer throughout society.

High quality infrared detectors that are capable of operating at more flexible temperature ranges allow for greater design flexibility in infrared sensing equipment. One prime example of limitations due to required cooling systems is the James Webb deep space telescope currently in production by NASA. This spacecraft has a limited lifetime due to its limited supply of coolant. One of the primary uses of this coolant is to reduce the temperature of the infrared detection systems aboard the telescope.

D.3 Impact of Research Results on the Environment

With increased societal interest in "green" technology, more efficient electrical devices and power production methods are required. Nanostructures could provide the next generation of solar cells and power-efficient electronics, thus reducing societal dependence on coal and other non-renewable fuel sources.

While the synthesis procedure utilized in this research is less costly than methods such as molecular beam epitaxy, it also produces much more chemical waste. This waste is toxic in nature, as it contains high levels of heavy metal elements, as well as carcinogenic compounds. This waste requires special disposal techniques and storage.

Appendix E: Microsoft Project for MS MicroEP Degree Plan

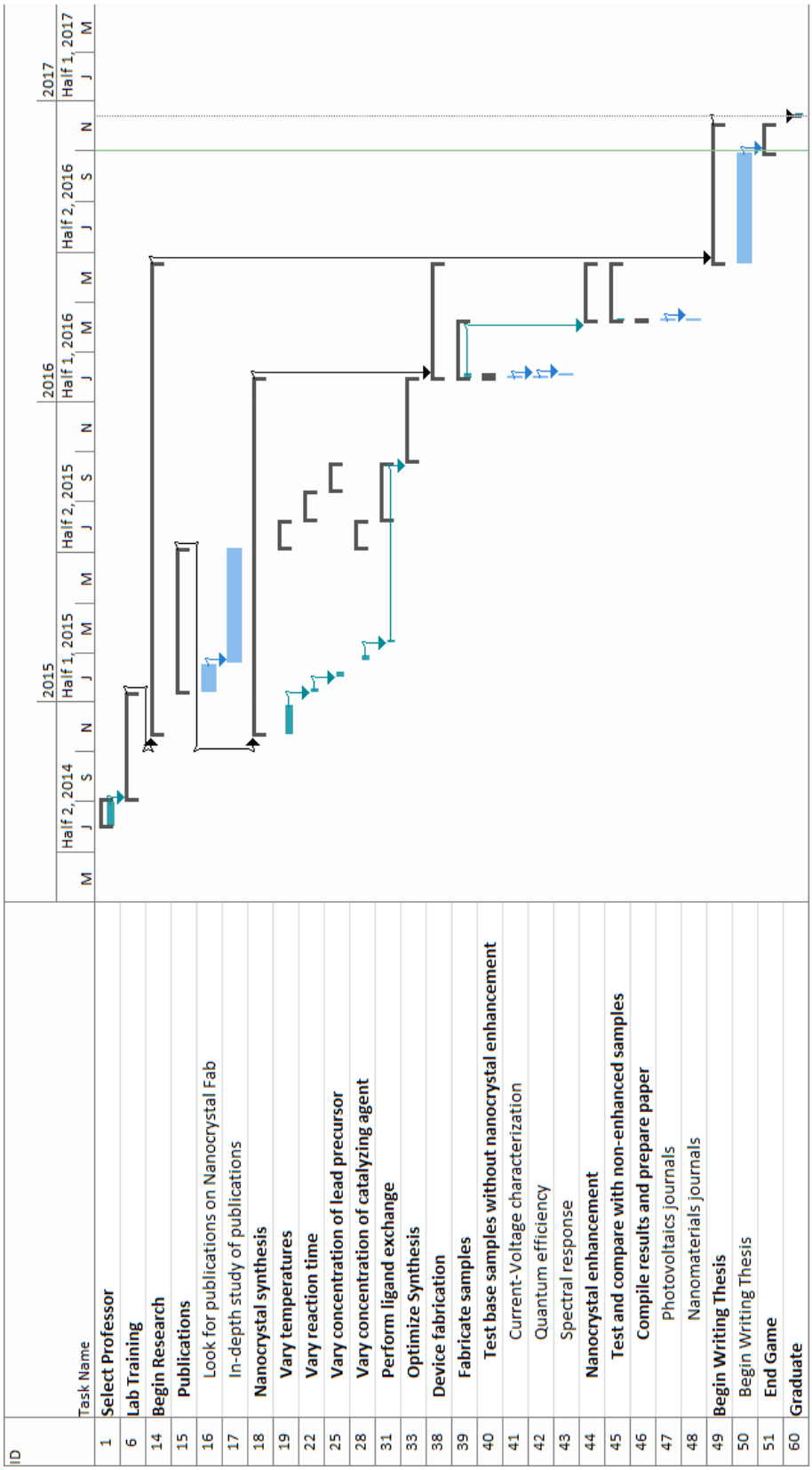

Appendix F: Identification of All Software Used in Research and Thesis

Computer #1:
- Model: Dell
- Serial Number: 8766882794
- Location: BELL 3143
- Owner: Dr. Omar Manasreh

Software #1:
- Name: Microsoft Word 2013
- Purchased by: UA Electrical Engineering

Software #2:
- Name: Origin 8.6
- Purchased by: Dr. Omar Manasreh

Software #3
- Name: Microsoft Excel 2013
- Purchased by: UA Electrical Engineering

Software #4
- Name: Microsoft Paint
- Purchased by: UA Electrical Engineering

Software #5
- Name: Mendeley Desktop
- Purchased by: None (Freeware)

Computer #2
- Model: Custom built
- Serial number: N/A
- Location: Personal computer
- Owner: Justin Hill

Software #1
- Name: Microsoft Word 2016
- Provided by: University of Arkansas

Software #2
- Name: Microsoft Excel 2016
- Provided by: University of Arkansas

Software #3
- Name: Microsoft Paint
- Purchased by: Justin Hill

Software #4
- Name: Mendeley Desktop
- Purchased by: None (Freeware)

Appendix G: All Publications Published, Submitted and Planned

A. Nusir, S. Member, J. Aguilar, J. Hill, H. Morris, M. O. Manasreh, and S. Member, “Uncooled Infrared Photodetector Utilizing PbSe Nanocrystals,” IEEE Trans. Nanotechnol., vol. 15, no. 1, pp. 109–112, 2016.